ESD-TR-75-329

Technical Note

1975-26

A Bandwidth Conserving Approach to Multiple Access Satellite Communication for Mobile Terminals

B. E. White
R. M. Mersereau

17 December 1975

Prepared for the Department of the Navy
under Electronic Systems Division Contract F19628-76-C-0002 by

Lincoln Laboratory
MASSACHUSETTS INSTITUTE OF TECHNOLOGY
LEXINGTON, MASSACHUSETTS

The work reported in this document was performed at Lincoln Laboratory, a center for research operated by Massachusetts Institute of Technology. The work was sponsored by the Department of the Navy under Air Force Contract F19628-76-C-0002.

This technical report has been reviewed and is approved for publication.

FOR THE COMMANDER

Eugene C. Raabe

Eugene C. Raabe, Lt. Col., USAF
Chief, ESD Lincoln Laboratory Project Office

MASSACHUSETTS INSTITUTE OF TECHNOLOGY
LINCOLN LABORATORY

A BANDWIDTH CONSERVING APPROACH TO MULTIPLE ACCESS SATELLITE COMMUNICATION FOR MOBILE TERMINALS

B. E. WHITE
Group 67
R. M. MERSEREAU
Consultant

TECHNICAL NOTE 1975-26

17 DECEMBER 1975

LEXINGTON MASSACHUSETTS

ABSTRACT

The problem of efficiently packing many mobile user signals into the available UHF uplink bandwidth of an advanced communications satellite is considered. It is assumed that the user terminals are mutually unsynchronized in timing, frequency and transmitter power control, and that the satellite performs the processing functions of tracking the symbol timing and Doppler shift of each user, demodulating the uplink signals, and reorganizing the information for the downlink. The basic approach is FDMA with QPSK modulated data streams individually modified by spectral shaping using data windows. BPSK and MSK modulation formats were also investigated.

From extensive computer simulations it is concluded that with relatively little degradation 20 unsynchronized 16 kbps satellite users can be packed into a 500 kHz uplink bandwidth that is shared with terrestrial LOS allocations. Alternatively, 7 unsynchronized 2400 bps users can occupy a 25 kHz bandwidth or 133 such users can be packed into a 500 kHz bandwidth. Signal strengths may vary by as much as 10 to 15 dB at the satellite without the need for transmitter power control. Peak-power-limited QPSK with a rate 1/2 convolutional code is slightly inferior to uncoded MSK for bit error rates larger than 10^{-3}. Spectrally shaped and coded QPSK, however, is needed for smaller error rates and will be more attractive if the modulator is not peak-power-limited.

TABLE OF CONTENTS

GLOSSARY

Abbreviations

AWGN	additive white Gaussian noise
CE	constant envelope
CPQFSK	continuous phase quadrifrequency shift keying
CT	crosstalk
CVSD	continuously variable slope delta (modulation)
DC	Dolph-Chebyshev
DFT	discrete Fourier transform
FFT	fast Fourier transform
GN	Gaussian noise
ISI	intersymbol interference
LOS	line-of-sight
MMSE	minimum mean-square error
MPSK	M-ary phase shift keying
MSK	minimum shift keying
PS	prolate spheroidal
QPSK	quadriphase shift keying
SNR	signal-to-noise ratio

Symbols

A_u	amplitude of user u
d_u	Doppler shift of user u
E	relative received power of interfering user
E_b	useful received signal energy per information bit
η	number of symbols spanned by transmitter window
F	input to ISI filter
f_c	nominal user bandwidth (center frequency to cutoff)
h_ζ	impulse response
H(z)	z-transform of impulse response
k_u	center frequency of user u
L_t	maximum received signal energy loss due to transmitter windowing
N	number of frequencies in digital analysis bandwidth
N_c	number of complex samples per symbol
N_d	symbol delay of MMSE filter
N_p	number of poles in MMSE filter
N_s	length of satellite window
N_t	length of transmitter window
n_u	delay of user u
N_w	window length
N_z	number of zeros in MMSE filter
N_o	single-sided noise power spectral density
ν	number of symbols spanned by satellite window

P_b	bit error probability
P_s	symbol error probability
$\phi_{st}(\ell)$	crosscorrelation of satellite and transmitter windows
$R_{\rho\sigma}(\ell)$	crosscorrelation of variables ρ and σ
s	satellite window
t	transmitter window
T_c	symbol interval
T_s	sampling interval
u	satellite user index
W_N	exp (-j $2\pi/N$)
x_ζ	transmitted symbol
X	output of ISI filter
ζ	symbol index

Notations

.*	complex conjugate of .
$\otimes$	convolution operation
$\overline{\cdot}$	ensemble average of .

I. SUMMARY

The subject of this report is modulation techniques for bandwidth conservation utilizing an advanced processing satellite envisioned for the 1980's.

1.1 Introduction

There is a need to provide efficient service to many mobile Ultra High Frequency (UHF) terminals operating in a frequency division multiple access (FDMA) uplink mode [1]. These terminals may be located on submarines, ships, aircraft, etc., operating anywhere on the surface of the earth. The terminals will operate at a variety of communication data rates [2]. Three representative data rates are 75 bits per second (bps) (teletype), 2400 bps (data or vocoded speech) and 16 kbps (continuously variable slope delta (CVSD) modulation voice [3, 4], which has a particularly simple implementation). Since the terminals will vary considerably in effective radiated power (ERP) the received signal powers at the satellite can differ by as much as 15 or 20 dB.

Because a large number of terminals is anticipated, the overall system cost dictates that the user terminals be relatively simple. Transmitter power control, symbol timing and Doppler correction all contribute to terminal complexity. It is generally desirable to shift the burden for realizing these functions to the satellite as much as possible in order to hold down the cost of a typical terminal.

Another concern is the problem of frequency allocation in the government UHF band (225 to 400 MHz). There are thousands of line-of-sight (LOS) users allocated at 100 kHz centers. In anticipation of more closely spaced allocations, there are a large number of terminals capable of tuning to 50 kHz centers and a smaller but growing number tunable to 25 kHz centers [5-7]. It is

unlikely that more than a few hundred kHz of contiguous bandwidth would be available for the allocation of satellite users. Thus, the uplink will probably be composed of a collection of sub-bands, each one of which might contain a number of satellite users and perhaps some LOS users as well.*

If a degree of anti-jam (AJ) protection is desired, these sub-bands could also be frequency hopped at a modest rate, e.g., 75 hops per sec to be compatible with the teletype rate. The problem of reacquiring phase at the receiver with each frequency hop, a difficulty that is present with coherent baseband modulation schemes, is not addressed in this report.

An FDMA uplink mode is an attractive candidate under these circumstances. Although certain frequency bands could actually contain time division multiple access (TDMA) traffic, this possibility will not be developed here. Two problems with TDMA are that the weaker terminals may not be able to support the burst rates required, and the terminals would have to be synchronized.

Looking toward the future in satellite communications it is reasonable to expect significant progress in on-board processing capabilities that would be reflected in upgraded service in several areas. Ten years from now a general purpose UHF satellite could provide at least 500 kbps of throughput data rate, which is an order of magnitude more capacity than will be available in the near term. Advanced modulation techniques would permit the more efficient use of the crowded UHF band. Separation of the uplinks and downlinks would result in greater system versatility emcompassing such features as more cross-

* Naturally, it is important that the satellite users and the LOS users do not interfere with one another. This issue will be addressed by the spectral shaping of the satellite user signals.

band operation between UHF and other frequency bands, selective treatment of different coverage areas on the earth, and uplink AJ protection at UHF.

Thus, the satellite itself is presumed to be an advanced processing satellite capable of demodulating the uplink signals, reorganizing the demodulated data for the downlink and remodulating the information according to the destinations specified. Such a satellite might employ multiple beam antennas, perform AJ antenna array nulling and frequency dehopping, participate in the tracking and correction of symbol timing and Doppler shifts for uplink users, and execute the multifarious control functions necessary for such versatile operation.

For the purpose of this report the satellite downlink may be thought of as either frequency division multiplexed (FDM) or time division multiplexed (TDM). The reasons for preferring one or the other downlink mode are beyond the scope of this report and will not be discussed.

The fundamental objective of this report is to establish a means for accomplishing the close frequency packing of more than the usual number of satellite users in a contiguous section of uplink bandwidth.

With the hope of achieving a minimum of terminal and satellite processing, this close packing could be attempted for unsynchronized users (for terminal simplicity) by carefully selecting an appropriate modulation scheme. The degree of packing would be limited by the center frequency separations required to reduce interuser interference to a tolerable level.

If the users were synchronized the modulated waveforms arriving at the satellite could be made orthogonal and the users could indeed be very closely

packed in frequency. Furthermore, there would be no power control problem because of the signal orthogonality. On the other hand, synchronization increases terminal complexity and systems dependent on sync may be fragile. Hence, it is desirable to consider the efficacy of the unsynchronized case.

With unsynchronized users there will generally be some crosstalk (CT) among the various received signals in the satellite demodulation channels. As a first step in attaining the close packing objective, the worst case CT between just two uncoordinated user signals has been calculated for eight different types of simple modems, including those utilizing binary phase shift keying (BPSK), a few variants of quadriphase shift keying (QPSK), and continuous phase frequency shift keying (CPFSK). These results are interesting in themselves but because of the rather restricted scope of the investigation it was decided to treat that subject in a separate but companion report [8]. However, the major conclusion of that study will be included in the next section of this report.

In this report the principal concern is with the more general situation where additional terminal and/or satellite processing is permitted. In particular, user signals may be either synchronized or unsynchronized in time and/or frequency. Spectral shaping of the transmitted and/or received signals will allow users to be closely spaced. The shaping is accomplished by digital filtering at either the terminal or the satellite or both.

The general system block diagram indicating the approach taken in this report is given in Fig. 1.1. Since most of the processing for bandwidth conservation is best accomplished digitally, and because the mathematics of analog

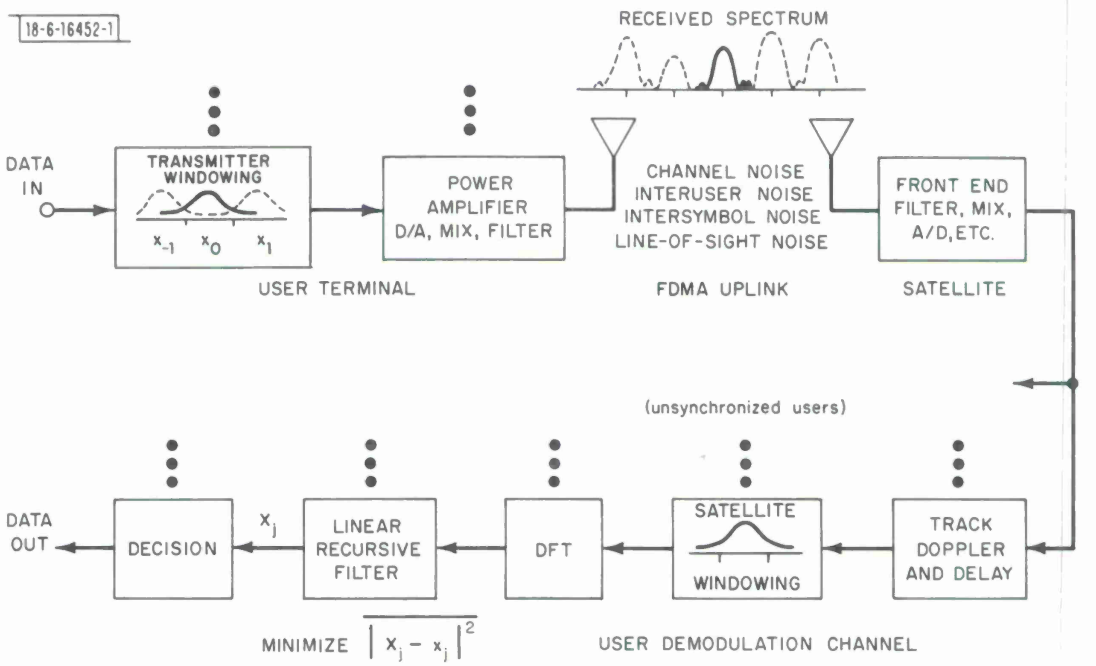

Fig. 1.1. Basic system approach for bandwidth conservation using data windows.

and digital processing are basically equivalent [9], very little will be said about the analog or digital to analog (D/A) portions of the system. The analog to digital (A/D) portion will be discussed briefly in Section 5.1. Specific options for this mix between analog and digital satellite processing, multiple front ends, intermediate frequencies (IF's), etc., can have a considerable impact on satellite design but these issues will be left for future study.

As seen in Fig. 1.1 just one contiguous section of user bandwidth is assumed. At some point in the satellite a digital baseband signal is obtained and fed to a number of replicated user demodulation channels, one channel for each user to be demodulated. Although the primary focus of this report is on a typical demodulation channel there will be an attempt to deal with some of the larger satellite processing questions involving synchronized versus unsynchronized users, timing and Doppler tracking, mixed data rates, etc.

In this report, it is assumed that the satellite tracks the symbol timing and Doppler of each user it demodulates without elaborating on how this might be done.

The essence of the windowing approach of this report will now be described. As depicted in Fig. 1.1 the filtering for spectral shaping is applied in the time domain by amplitude weighting (windowing) the signals at the transmitter and satellite with data windows. The desired weighting coefficients can be generated easily with digital read only memories (ROM's) and D/A converters. For the problem considered here, this is more efficient than convolutional filtering [10 - 12]. In addition, data windows are finite in extent which enables the windows to be applied without introducing intersymbol interfer-

ence (ISI). ISI, when introduced by windowing over more than one information symbol as shown in Fig. 1.1, can be easily mitigated. As will be seen the ISI is specified by the crosscorrelation function of the satellite and transmitter windows.

Windowing at the terminal controls the spectrum of the transmitted signal so that there is less spectral splatter from one satellite user to another. Transmitter windowing will also reduce the crosstalk (CT) between a satellite user and a line of sight (LOS) user in the vicinity of the transmitting satellite user. Windowing at the satellite reduces out of band interference and restricts the demodulation bandwidth for a given satellite user. If the spectral window at the satellite is sufficiently narrow, it will also reject the signal from an LOS user at the band edge. In general, the longer the data windows the more effective the spectral shaping will be and the less the CT. On the other hand, longer windows generally mean increased ISI. Transmitter windowing may also imply non-constant envelope signaling which for peak-power-limited transmitters means a received signal energy penalty with respect to channel noise. So in this model of the FDMA environment, there are four sources of error — the usual channel noise, assumed to be additive white Gaussian noise (AWGN), CT among users, ISI, and LOS interference. Clearly, there will be system design tradeoffs among these four sources of interference.

There are many ways to mitigate ISI in the presence of AWGN. In relation to most situations covered in the literature [13 - 23], the ISI problem at hand is rather a mild one since the ISI is deliberately introduced (hence, known),

of limited extent and time-invariant. As will be shown in this report, the ISI that arises in controlling CT from closely packed users can be effectively eliminated with a simple digital filter. As indicated in Fig. 1.1 the filter can be designed to minimize the mean square error (MSE) between the input to the decision device in the satellite and the actual symbol transmitted. The resulting filter is suboptimum in the sense that the probability of a symbol error is not actually minimized. However, it is also shown through computer simulation that the filter performs nearly identically, at least down to 10^{-3} bit error rates, to the more complex Viterbi algorithm implementation which realizes a maximum likelihood detection on the entire transmitted sequence.

Being identical in design the ISI filters and decision devices could be either replicated or time shared among user demodulation channels.

Presumably some combination of partially coherent [24 - 28] or differentially coherent [29, 30] detection will be employed in an actual implementation. The theoretical and experimental degradations from coherent performance in AWGN are well established [31, 32] and can be used in a more refined analysis. For simplicity and concreteness only coherent matched filter hard decision receivers [33] are considered in this report.

The baseline modulation scheme employed is QPSK [34], although some of the computer simulated results obtained may apply equally well to offset QPSK [35, 36] and M-ary PSK. Simulation has also been performed for BPSK and minimum shift keying (MSK)* [37 - 39]. Some related work dealing with up to two interfering QPSK user signals is found in [40, 41].

---

* Binary continuous phase FSK with a frequency deviation ratio of 1/2.

Coding issues are secondary to modulation techniques for bandwidth conservation and are not considered with much detail in this report. However, it is recognized that coding may be necessary to achieve the required system performance especially when considering all types of interference. Convolutional coding [42] can be a particularly efficient means of improving performance with a reasonable increase in system complexity. At present, coding is usually considered to be end-to-end in nature, i.e., no uplink decoding or re-encoding for the downlink in the satellite. For convenience in evaluating the uplink performance with coding, decoding is assumed to take place in the satellite, or alternatively, downlink noise is neglected. This analytical device affects the performance level only slightly and has very little bearing on the conclusions of this report which are presented in the next section.

The rest of the report is organized as follows. Section II contains a description of the mathematical model of the system and an analysis of ways to mitigate intersymbol interference introduced by the spectral shaping. Section III discusses data windows which produce the spectral shaping for controlling crosstalk among closely packed user signals. Simulated results of various system designs are presented in Section IV. Finally, Section V discusses some implementation issues bearing on system complexity. A glossary and a representative list of references are provided in this report to assist the interested reader.

1.2 Conclusions

The overall results of this report and its companion [8] are discussed in this section. The major conclusions are capitalized for emphasis.

The principal conclusion of the companion report where crosstalk (CT) among users is combatted simply by sufficient center frequency separation of the modulated waveforms with no in-band filtering (See Table 1.1) is that:

WITH NO SPECIAL PROCESSING, I.E., NO WINDOWING,
MANY MORE CONTINUOUS PHASE FSK USERS CAN OCCUPY
A GIVEN BANDWIDTH THAN EITHER BPSK OR QPSK USERS.

A worst case analysis assuming hard decision coherent receivers suggests that three to five times as many minimum shift keyed (MSK) waveforms as QPSK waveforms within a specified bandwidth are possible at a tolerable level of CT interference. The bandwidth advantage of MSK over the variants of QPSK was shown to increase with the power level of the interfering waveforms.

At this point a brief explanation of this behavior is worthwhile. An MSK signal is a continuous waveform that can be detected with the same bit error probability in AWGN as BPSK or QPSK. The phase continuity of MSK results in a very compact signal spectrum with a rapidly decreasing sidelobe level as a function of frequency. Although the bandwidth between the principal spectral nulls of MSK is 50% larger than that of QPSK for random data at the same rate, the fraction of out-of-band energy is generally much smaller for MSK than for QPSK. It has been determined that the crosstalk decreases only linearly with center frequency separation with M-ary PSK while with continuous phase FSK the CT dependence varies as the inverse square of the frequency separation. This is consistent with the asymptotic behavior of the various spectra. The reader is referred to the companion report [8] for more details.

Later in this section the number of user signals possible in a given bandwidth, and at a certain data rate and performance level, both with a without

windowing, will be estimated. Naturally, a greater density of waveforms will be possible using the special windowing techniques of this report. Subsequent discussion will focus on the conclusions that arose from this additional signal processing for bandwidth conservation.

In this discussion the modulated waveforms transmitted by the satellite users are nominally identical in form and spectrally located at closely packed but distinct center frequencies. Either QPSK or MSK modulation is assumed with a user data rate of 16 kbps and a center frequency spacing of 25 kHz. Except for a slight degradation due to Doppler shifts the system performance for data rates of 2400 bps and frequency spacings of 3750 Hz is essentially unchanged except for the scaling factor in time and frequency. Since the effects of Doppler shifts may dominate at 75 bps, the close packing of user signals at the teletype rate will not be addressed in this report.

Typically the uplink bandwidth will be composed of a collection of subbands each 500 kHz wide, say, containing 20 16 kbps satellite users and also some interfering LOS users. Supposing that the LOS users produce narrowband spurious interference they are modeled as narrowband-filtered AWGN at 25 kHz centers. The satellite users are still located 25 kHz apart but in between and at least 12.5 kHz from each LOS user.

Because of the natural compactness of the MSK spectrum, windows were applied at the transmitter only to the PSK waveforms. With transmitter windowing there are two separate cases to consider depending on whether the transmitter is or is not peak-power-limited. If a non-rectangular window is applied

and the transmitter is already operating at full power, then there will be a signal energy loss relative to the channel noise at the receiver. The loss is determined by the ratio of the energy in the window to the energy in a rectangular window of the same length. Simulated results for QPSK will be presented assuming such a peak-power limitation, and just for one particular data window, for which this loss happens to be 3.07 dB. That is, the transmitter power required to achieve a certain error probability and E_b/N_o with QPSK will be up to about 3.1 dB more under a peak-amplitude restriction. There will be no such loss associated with the constant envelope MSK waveforms since a transmitter window is not applied.

Windows were applied at the satellite to both QPSK and MSK waveforms. In contrast to the QPSK case, when a satellite window was applied to MSK, it was done in such a way that no intersymbol interference was introduced.

Symbol error probabilities down to 10^{-3} were measured by computer simulation for uncoded QPSK at 16000 4-ary symbols per sec and uncoded MSK at both a 16 kbps and 32 kbps binary symbol rate. The rate 1/2 coded performance of QPSK was estimated by the technique explained in Section 4.5. The larger MSK bit rate, corresponding to a rate 1/2 code, proved to be infeasible for the 25 kHz user spacings, so coded MSK performance was not estimated. Uncoded MSK at the 16 kbps rate performed quite well, however. Thus, the performance of uncoded MSK and coded QPSK will be compared on the common basis of a 16 kbps information rate and a 25 kHz user separation.

The required E_b/N_o's for a coherent receiver and three different reliability levels are listed in Table 1.1. The parameter E refers to the received power

TABLE 1.1

SIMULATED COHERENT PERFORMANCE WITH WINDOWING AND ADJACENT LOS USERS FOR CODED QPSK* AND UNCODED MSK

a. E = 10 dB

Bit Error Probability	E_b/N_o Required			Degradations from Theoretical for AWGN		
	QPSK		MSK	QPSK		MSK
	3-Bit Decisions	Hard Decisions		3-Bit Decisions	Hard Decisions	
$< 10^{-2}$	3.3 dB	5.7 dB	5.4 dB	0.8 dB	1.6 dB	0.2 dB
$< 10^{-3}$	4.5 dB	7.2 dB	9.2 dB	1.3 dB	2.1 dB	1.9 dB
$< 10^{-5}$	6.8 dB	9.0 dB	-	2.0 dB	2.4 dB	-

b. E = 15 dB

Bit Error Probability	E_b/N_o Required			Degradations from Theoretical for AWGN		
	QPSK		MSK	QPSK		MSK
	3-bit Decisions	Hard Decisions		3-bit Decisions	Hard Decisions	
$< 10^{-2}$	4.2 dB	8.6 dB	6.8 dB	1.8 dB	4.5 dB	1.6 dB
$< 10^{-3}$	6.1 dB	12.3 dB	10.4 dB	2.9 dB	7.2 dB	3.1 dB
$< 10^{-5}$	11.1 dB	-	-	6.3 dB	-	-

* Because QPSK requires a transmitter window, up to 3.1 dB more transmitter power is needed for QPSK than MSK for a given E_b/N_o if the transmitter is peak-power-limited.

level of every other satellite user signal relative to the user signal being demodulated. LOS users were located on either side of the demodulated satellite user and were about 11 dB above a peak-power-limited satellite user in pre-filtered mean-square signal amplitude.

Coded QPSK results are presented for both 3-bit soft-decision and 1-bit hard-decision demodulation in the satellite. 3-bit decisions have an advantage of at least 1/2 dB and 2 dB over 2-bit soft-decision and hard-decision demodulation, respectively, for the convolutional code employed [42]. With soft-decision demodulation in the satellite and end-to-end coding the downlink bandwidth necessary will generally exceed the uplink bandwidth utilized. More satellite power may also be required. The additional downlink power and bandwidth required would depend on many factors including the modulation format, signaling alphabet size, power budget margin, etc., for the downlink and therefore will not be treated in this report. If it turns out that insufficient downlink power or bandwidth is available for soft-decisions and end-to-end coding then either hard-decision demodulation or in-satellite decoding must be used with QPSK.

Observe from Table 1.1 that:

> CONSIDERING THE ADDED 3.1 dB TRANSMITTER POWER REQUIRED FOR WINDOWED QPSK UNDER A STRICT PEAK-POWER LIMITATION AT THE TRANSMITTER, MSK IS BETTER THAN CODED QPSK FOR CVSD MODULATED VOICE ($P_b < 10^{-2}$), EVEN FOR SOFT-DECISION DEMODULATION, AND FOR VOCODED SPEECH ($P_b < 10^{-3}$) FOR HARD-DECISION DEMODULATION.

MSK has the additional advantages of constant envelope signaling and not requiring ISI rejection filters and coding equipment. Constant envelope sig-

naling was not possible for QPSK at an acceptable performance level except with near perfect power control (E = 0 dB).

For the smaller error probabilities of Table 1.1:

> CODED QPSK WITH SOFT DECISIONS IS BETTER THAN MSK FOR VOCODED SPEECH ($P_b < 10^{-3}$) OR DATA TRANSMISSIONS ($P_b < 10^{-5}$). CODED QPSK WITH HARD DECISIONS SHOULD OUTPERFORM MSK FOR $P_b < 10^{-5}$ AND E = 10 dB INTERFERING USERS, EVEN WITHOUT A PEAK-POWER LIMITATION AT THE TRANSMITTER.

Although accurate performance estimates below $P_b = 10^{-5}$ are lacking for MSK and for hard-decision QPSK at E = 15 dB, it is unlikely that MSK could outperform QPSK at the assumed frequency spacings even with transmitter windowing and higher rate codes. Coded QPSK with soft decisions would be substantially better than MSK under no peak-power limitation. Unfortunately, the performance advantage is not easily estimated.

Also, from the performance figures in Table 1.1:

> WITH NO PEAK-POWER LIMITATION AT THE TRANSMITTERS, CODED QPSK WITH SOFT-DECISIONS IS SUPERIOR TO MSK BY AT LEAST 2 dB FOR $P_b < 10^{-2}$, AND AT LEAST 4 dB FOR $P_b < 10^{-3}$, WHILE CODED QPSK WITH HARD DECISIONS IS 2 dB BETTER THAN MSK FOR $P_b < 10^{-3}$ AND E = 10 dB INTERFERING USERS BUT WORSE THAN MSK BY ABOUT 2 dB FOR E = 15 dB.

In summary, then:

> WITH THE RELIABILITY LEVELS AND PERFORMANCE DEGRADATIONS OF TABLE 1.1: 20 UNSYNCHRONIZED 16 kbps SATELLITE USERS CAN BE PACKED INTO A 500 kHz UPLINK BANDWIDTH INCLUDING NARROWBAND LOS USERS AND COMMUNICATE SIMULTANEOUSLY IN AN FDMA SATELLITE MODE OF OPERATION. THE RECEIVED SIGNAL STRENGTHS MAY VARY BY

10 TO 15 dB WITHOUT THE NEED FOR TRANSMITTER POWER CONTROL. BY SCALING THESE RESULTS UP TO 7 UNSYNCHRONIZED 2400 bps USERS SPACED BY 3750 Hz CAN OCCUPY A 25 kHz BANDWIDTH OR AS MANY AS 133 SUCH USERS CAN COMMUNICATE IN A 500 kHz BANDWIDTH.

In view of the worst case crosstalk analysis for the close packing of MSK waveforms without windowing [8], this is approximately twice the number of users possible in these bandwidths without the special processing techniques developed in this report.

It should be emphasized that computer simulations were performed with a reasonable but quite specific model for LOS interference (see Section IV). However, the techniques of this report should be useful in dealing with other LOS models. For example, a longer satellite window and/or a sharper cutoff frequency could be used against stronger and/or wider band LOS interference. The net increase in residual intersymbol interference may be tolerable, particularly in situations where transmitter windowing is not required. This may be the case when a single satellite user is allocated a small portion of a bandwidth occupied predominantly by LOS users.

II. Analysis

2.1 Mathematical Model for an MPSK Digital System

In this section a mathematical model for the signal processing parts of an M-ary PSK system is presented and some terminology is established which will be used throughout this report. Since MSK modulation does not quite fit this model and is not considered with as much generality as MPSK in this report, the mathematical model for MSK will be treated separately in Section 2.4.

Figure 2.1 depicts a digital equivalent model for an MPSK system which omits the analog and hybrid parts of a real system such as the analog to digital converters, analog modulators, etc. Referring to that figure let ζ be the input symbol index for a typical user u. The complex sequence of input symbols to user u, $x_{u\zeta}$, is converted into a sequence $y_u(n)$ of complex numbers by using a transmitter data window t(n) which is common to all users. As an example, t(n) might be a sequence of constant height (referred to as the rectangular window) which spans the interval between the arrival of $x_{u\zeta}$ and $x_{u,\zeta+1}$. This particular window has the distinct advantage of permitting constant envelope signaling for a user with a peak-power-limited transmitter, but on the other hand this window does little spectral shaping and thus produces potentially serious inter-user interference or crosstalk (CT). In the more general case, $y_u(n)$ will not have a constant envelope and the window t(n) will span more than one symbol interval in order to reduce the spectral splatter of user u in the frequency bands of other users. However, windows that span more than one symbol interval introduce intersymbol interference (ISI). In designing a good window, the minimization of CT, the minimization of ISI and producing a signal with a nearly constant envelope are conflicting objectives. This will become clearer in

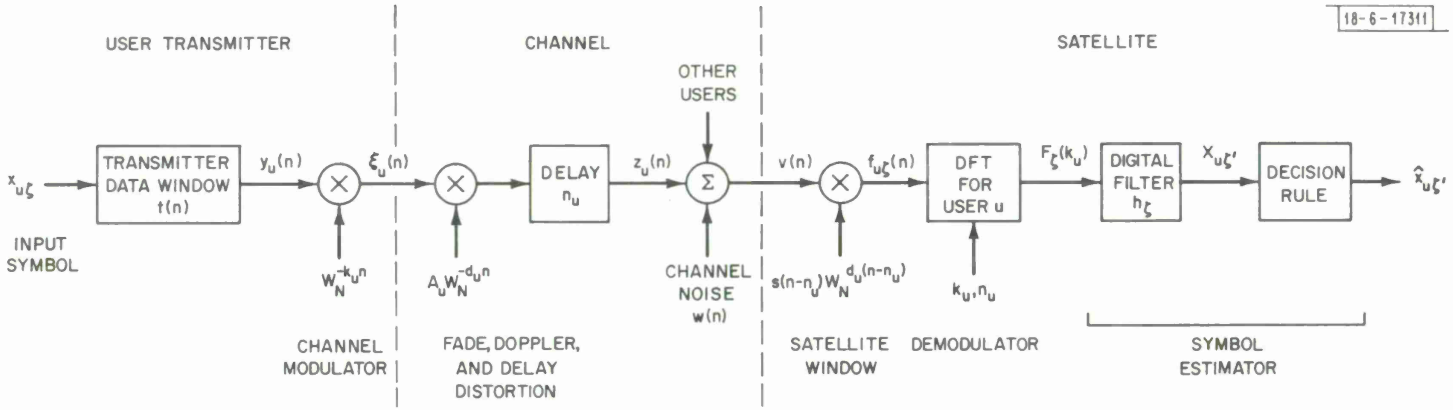

Fig. 2.1. MPSK digital system model (only one user path is shown).

what follows.

The sequence $y_u(n)$ is modulated by the sequence $W_N^{-k_u n}$, where N is the number of discrete frequencies in the digital analysis bandwidth $W_N = \exp(-2\pi j/N)$ with $j = \sqrt{-1}$, and k_u is an integer between 0 and $N - 1$ corresponding to the carrier frequency for user u. The modulated signal is then converted into a continuous signal by an analog to digital converter (complex), further modulated by an uplink carrier, transmitted over a (presumed) additive white Gaussian noise (AWGN) channel, demodulated to an intermediate frequency (IF) and re-sampled. This whole section of the system can be modeled as a digital channel.

In this channel the user's signal is delayed by a delay n_u with respect to the other users (since all users are at different distances to the satellite) and attenuated to a real amplitude A_u. The user's frequency is also perturbed by an amount d_u due to Doppler shifts caused by relative motion between the transmitter and satellite. In the channel the perturbed signal is, of course, also combined with similarly modified signals of other satellite users, spurious signals from line-of-sight (LOS) users and with AWGN. For the purpose of this model and the simulation of Section IV, the delay and Doppler shift of each satellite user are fixed random variables, i.e., n_u and d_u are randomly selected at the start of an experiment but held constant for the duration of a simulation run.

The transmitted signal is thus perturbed in the channel to form the modified user sequence

$$z_u(n) = A_u y_u(n - n_u) W_N^{(k_u + d_u)(n_u - n)} \tag{2.1}$$

where A_u is a real amplitude, d_u is a Doppler shift and n_u is a propagation

delay. The AWGN sequence will be denoted by w(n) and the total received sequence at the satellite will be denoted by v(n).

At the satellite the signals are demodulated. It is anticipated that this will be accomplished in U distinct demodulation channels and that due to tracking, the center frequency k_u, Doppler shift d_u, and delay n_u for each user signal will be available at the satellite. In the special case that the user Doppler shifts and delays are precorrected so that the effective Doppler shifts and delays are zero, then the demodulation can be performed on all of the channels simultaneously.

The input data stream at the satellite is segmented into subsequences of length N_w by means of a satellite data window, s(n). In addition the satellite window provides further spectral shaping to help reduce crosstalk and reject LOS interference. This window is applied once per symbol interval on each demodulation channel. It is modified to compensate for the Doppler shift d_u and it is delayed so that it is applied at the beginning of each symbol interval. If $f_{u\zeta}(n)$ denotes the output sequence from the windowing operation then

$$f_{u\zeta}(n) = s(n - n_u)\ v(n)W_N^{d_n(n - n_u)}, \quad n_u \leq n \leq N + n_u - 1 \quad . \quad (2.2)$$

As a practical matter it may be noted that the multiplication by $W_N^{d_u(n - n_u)}$ in Eq. (2.2) need be performed only for those users with significant Doppler shifts.

In the special case $s(n) = t^*(n)$ the satellite and transmitter data windows are matched and the satellite window then functions as a matched filter. Thus in this case the signal-to-noise ratio at the output of the DFT is maximized.

A discrete Fourier transform (DFT)* is performed once each symbol interval for each user to separate the u-th signal from the others. When the parameters of the DFT are properly chosen, one obtains as the k_u-th output of the DFT an estimate of the input symbol $x_{u\zeta}$ for user u and input symbol interval ζ:

$$F_\zeta(k_u) = \sum_{n=n_u}^{N-1+n_u} f_{u\zeta}(n) W_N^{(n-n_u)k_u} = \sum_{n'=0}^{N-1} f_{u\zeta}(n' + n_u)\, W_N^{n'k_u} \quad . \qquad (2.3)$$

Note that some form of data window of length N is implicitly associated with the DFT since the DFT input must be of finite length. If the users are all synchronized in both time and frequency at the satellite, s(n) can be applied just once per symbol for all users and the DFT's needed for demodulation can all be performed simultaneously using a fast Fourier transform (FFT) algorithm with some savings in the processing hardware (and time) required.

The output of the DFT may or may not represent a good approximation to $x_{u\zeta}$ depending upon the windows chosen and the noise level in the channel. Windows that are longer than the intersymbol distance introduce ISI much of which can be removed by a simple digital filter at each DFT output. Such a filter,

---

* Technically this is non-standard terminology. The DFT is normally defined as:

$$F(k) = \sum_{n=0}^{N-1} f(n) W_N^{nk} \quad , \; k = 0, 1, \ldots, N-1 \quad .$$

In general it converts an N-point sequence into another N-point sequence. In this report the above sum is often computed for a single value of k, an operation which will be called a DFT for the lack of a better term. The fast Fourier transform (FFT) algorithm computes this sum for all N values of k simultaneously.

with impulse response h_ζ, produces a complex number $X_{u\zeta'}$, for each input $F_\zeta(k_u)$, where $\zeta - \zeta'$ is the symbol delay of the filter. Thus, the output symbol $\hat{x}_{u\zeta'}$ is an estimate of the earlier transmitted input $x_{u\zeta'}$.

The data windows t(n) and s(n) are restricted to be finite length real discrete time functions for a less complex implementation and to limit the extent of the ISI. It is assumed that the transmitter and satellite windows extend over at most an integral number η and ν of symbol intervals, respectively, and that their support is contiguous and centered with respect to those intervals. These assumptions do not appear to limit system performance significantly. Let N_t and N_s denote the length of t(n) and s(n), respectively, and let N_c be the intersymbol distance. ISI will be introduced whenever either window is longer than the intersymbol distance ($N_t > N_c$ or $N_s > N_c$).

One way to conceive of the operation of applying the transmitter window is to first generate a sequence $x_u(n)$ from the $x_{u\zeta}$ such that

$$x_u(n) = \begin{cases} x_{u\zeta}, & \text{for } n = \zeta N_c \\ 0, & \text{otherwise} \end{cases} . \tag{2.4}$$

The sequence $x_u(n)$ is thus a pulse train with the pulses spaced by N_c, the input symbol separation. An element in the sequence $y_u(n)$ is then the convolution of $x_u(n)$ and t(n). This procedure is illustrated in Fig. 2.2. Mathematically, $y_u(n)$ can be written as

$$y_u(n) = \sum_r x_{u,\zeta+r} \cdot t(n - rN_c) \tag{2.5}$$

All but η of the terms in the sum (2.5) will be identically zero for any n due

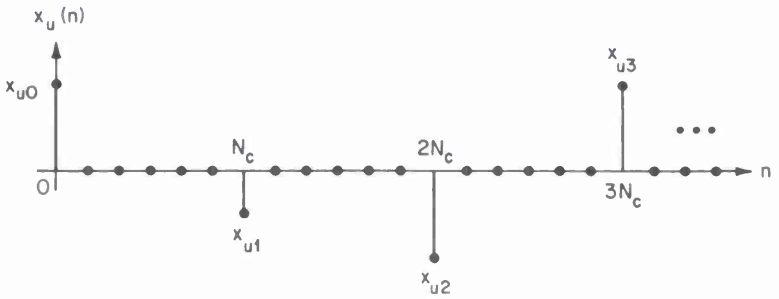

a. A complex signal $x_u(n)$.

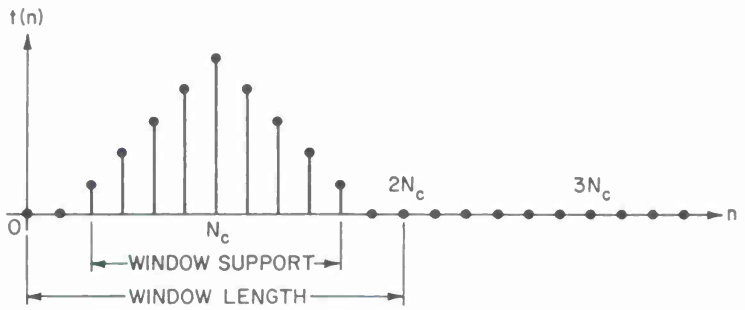

b. A real transmitter window t(n).

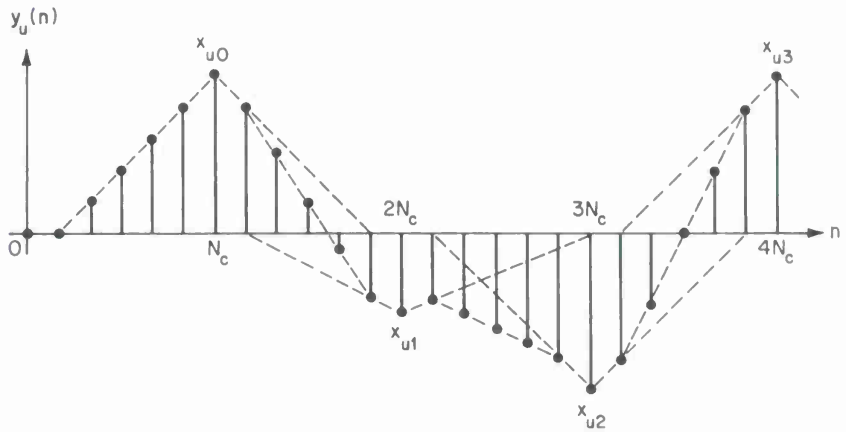

c. The complex transmitted signal $y_u(n)$.

Fig. 2.2. Transmitter windowing.

to the finite length of t(n).

2.2 Effects of Transmitter Windowing

In this section several properties of the transmitter window are discussed.

First, it is noted that for equimagnitude symbols, $|x_{u\zeta}| = 1$, say, constant envelope signaling is possible only for a rectangular transmitter window that spans exactly one symbol interval. A rectangular window of greater support results in non-constant envelope transmission, as can be deduced from Eq. (2.5).

The ηN_c-point DFT of an N_t-point rectangular transmitter data window of height h is given by

$$T(k) = h \frac{\sin\left(\frac{\pi N_t}{\eta N_c} k\right)}{\sin\left(\frac{\pi}{\eta N_c} k\right)} \exp\left(-j \frac{\pi(N_t-1)}{\eta N_c} k\right) \quad , \; k = 0, 1, \ldots, \eta N_c - 1 \quad . \tag{2.6}$$

A graph of $|T(k)|$ reveals that by modifying the value of N_t the magnitude and width of the main lobe of the function can be altered but little control over the sidelobes is available. Hence, only limited control over the interference among users is possible with this window. Furthermore, making the window longer by increasing N_t beyond N_c increases ISI. Using a more general shaped window one can improve both the spectral shaping due to the window for reducing CT, and the ISI, but this must be done at the expense of the signal energy for a peak-power-limited transmitter. Since the signal-to-noise ratio is reduced with a shaped window, the probability of error due to the AWGN in the channel increases. There are thus four sources of error: line-of-sight (LOS) interference, Gaussian channel noise (GN), crosstalk (CT), and intersymbol

interference (ISI). By varying window shapes and lengths, one can find various operating points which trade off the relative mix of these sorts of errors. When choosing windows, however, all four sources of error must be kept in mind.

Consider next the average signal energy penalty for a peak power limited transmitter in AWGN with a non-rectangular window. Assuming statistically independent zero-mean input symbols the total mean received signal energy from user u during one symbol interval is

$$E_{uc} = A_u^2 \, \phi_{tt}(0) \tag{2.7}$$

where

$$\phi_{st}(\ell) = \sum_{m=0}^{N_s-1} s(m) \; t(m - \ell N_c) \qquad \ell = 0, \pm 1, \pm 2, \ldots \tag{2.8}$$

is the crosscorrelation function between the two windows, and the shift is measured in symbols.

Clearly, for fixed A_u, N_t, N_c and for a transmitter window which is peak-amplitude-limited with amplitude h, the window yielding the largest mean energy is rectangular with constant amplitude h. The mean received energy from user u for such a window is

$$E_u = N_t (A_u h)^2 \tag{2.9}$$

by Eqs. (2.7) and (2.8). It is convenient to choose h such that $E_u = A_u^2$, i.e., so that for the rectangular window of support N_t, $\phi_{tt}(0) = 1$. With any other window, the energy received from user u will be less. In fact with this normalization the average fraction of energy received from user u with respect to E_u is simply $E_{uc}/E_u = \phi_{tt}(0) \leq 1$ from Eqs. (2.8) and (2.9). Thought of another

way, there is at most an

$$L_t = -10 \log_{10} \phi_{tt}(0) \text{ dB} \tag{2.10}$$

loss in mean received signal energy due to normalization at a peak-power-limited transmitter. For most of the non-rectangular windows tried in the simulation L_t was in the range 1.89 to 3.07 dB.

2.3 Combatting Intersymbol Interference

There are a number of ways to handle ISI, and there is a vast literature dealing with time-varying dispersive channels. However, because of the rather special nature of the ISI which appears here, a simple linear recursive filter of low order is used to reduce ISI [23,43,44]. The approach is suboptimal, but its performance in this context compares favorably with the optimal approach using the Viterbi algorithm, and it is much simpler to implement. Because this scheme was so simple and yet performed nearly optimally, other schemes were not tried since there seemed to be little to gain from alternate approaches [23,45,46].

A reasonable and tractable criterion for designing the digital filter of Fig. 2.1 is that of minimizing the mean-square error (MSE)

$$\varepsilon_{u\zeta} = \overline{|X_{u\zeta} - x_{u\zeta}|^2} \tag{2.11}$$

between the complex filter output symbol $X_{u\zeta}$ for user u and the corresponding system input symbol $x_{u\zeta}$. In fact, one is really interested in minimizing the decision error probability for a given signal-to-noise ratio. But this is a much more difficult if not intractable analytical task. Another approach might be to design the digital filter to maximize the signal-to-noise ratio (SNR) at the filter output. This latter approach has been tried but for typical

interference models (delays, Doppler shifts and amplitudes) the optimum SNR and minimum MSE (MMSE) filters are not significantly different.

Although the digital filter design will be based on the MMSE criterion, system performance will be measured by computer simulation to estimate decision error probabilities. A comparison will be made between the suboptimal MMSE filter and the optimal Viterbi algorithm approaches for reducing ISI. Although theoretical receiver operating characteristics are known for the Viterbi algorithm in AWGN, the formulas are not easily applied so performance will also be measured by simulation.

2.3.1 MMSE Recursive Filter Design

The MMSE digital filter that operates once per channel symbol to reduce ISI is designed as follows. For simplicity the subscript u's are temporarily deleted. If F_ζ denotes the input to the filter and X_ζ denotes its output, the filter is defined by the difference equation

$$X_\zeta = \sum_{i=0}^{N_z} \alpha_i F_{N_d + \zeta - i} + \sum_{i=1}^{N_p} \beta_i X_{\zeta - i} \quad . \tag{2.12}$$

F_ζ comes from Eq. (2.3) and includes the effects of crosstalk (CT). The filter design problem is the problem of finding the $\{\alpha_i, \beta_i\}$. In general these parameters can be complex but if the data windows are real, the $\{\alpha_i, \beta_i\}$ must be real. $N_d \geq 0$ is the filter symbol delay. N_z and N_p are the number of zeros and poles, respectively, of the digital filter.

Differentiation of Eq. (2.11) with respect to each α_i and β_i using Eq. (2.12) and setting each partial derivative to zero yields the nonlinear system of equations

$$\sum_i \alpha_i (R_{FF}(i-\ell) + R_{FF}(\ell-i)) + \sum_i \beta_i (R_{XF}(\ell-N_d-i) + R_{FX}(N_d+i-\ell))$$

$$= (R_{xF}(\ell-N_d) + R_{Fx}(N_d-\ell)), \quad \ell = 0,1,\cdots,N_z \tag{2.13a}$$

$$\sum_i \beta_i (R_{XX}(i-m) + R_{XX}(m-i)) + \sum_i \alpha_i (R_{XF}(i-N_d-m) + R_{FX}(N_d+m-i))$$

$$= (R_{xX}(m) + R_{Xx}(-m)), \quad m = 1,2,\cdots,N_p \tag{2.13b}$$

where $R_{\rho\sigma}(j-k) = \overline{\rho_j \sigma_k}^*$ [47] for the complex random variables ρ and σ. These equations are nonlinear because the correlation functions $R_{XX}(\ell)$, $R_{XF}(\ell)$, $R_{FX}(\ell)$, $R_{xX}(\ell)$ and $R_{Xx}(\ell)$ are themselves all functions of the $\{\alpha_i, \beta_i\}$. The fact that the windows and the $\{\alpha_i, \beta_i\}$ are real guarantees that all of the correlation functions in Eq. (2.13) are real functions of ℓ. Since for any correlation function $R_{\rho\sigma}(\ell) = R^*_{\sigma\rho}(-\ell)$ the equations of (2.13) can be simplified to the following:

$$\sum_i \alpha_i R_{FF}(\ell-i) + \sum_i \beta_i R_{FX}(N_d+i-\ell) = R_{Fx}(N_d-\ell), \quad \ell = 0,1,\cdots,N_z$$

$$\sum_i \alpha_i R_{FX}(N_d+m-i) + \sum_i \beta_i R_{XX}(m-i) = R_{Xx}(-m), \quad m = 1,2,\cdots,N_p. \tag{2.14}$$

It should be noted that the matrix of coefficients in Eq. (2.14) is symmetric, considering the $\{\alpha_i, \beta_i\}$ as unknowns.

The nonlinear equations of (2.14) were solved iteratively. First the system of linear equations

$$\sum_i \alpha_i R_{FF}(\ell-i) = R_{Fx}(N_d - \ell), \quad \ell = 0, 1, \ldots, N_z \tag{2.15}$$

was solved to give an initial vector $\underline{\alpha}^{(0)} = \{\alpha_0^{(0)}, \alpha_1^{(0)}, \ldots, \alpha_{N_z}^{(0)}\}$. Using the digital filter impulse response $h_\ell^{(0)}(\underline{\alpha}^{(0)}, \underline{\beta}^{(0)} = \underline{0})$ new correlation functions were then computed and the full set of Eqs. (2.14) was solved for $\underline{\alpha}^{(1)}$ and $\underline{\beta}^{(1)}$. The filter $h_\ell^{(1)}(\underline{\alpha}^{(1)}, \underline{\beta}^{(1)})$ was then used to compute a new set of coefficients $\underline{\alpha}^{(2)}$ and $\underline{\beta}^{(2)}$, and so on. Excellent convergence of the $\{\alpha_i, \beta_i\}$ has been observed within just a few iterations (typically 3 to 10).

Filters were computed for several values of N_p, N_z and N_d and $E_b/N_o + L_t^* = 10$ and 13 dB, where E_b is the mean received energy per bit from user u and N_o is the power spectral density of the complex zero-mean AWGN process. Good results were usually obtained for $N_z = 2$ to 4 and $N_p = 0$ or 1. Only very slight improvement was observed for larger values of N_z or N_p (consistent with [23]).

Thus, very simple linear filters are adequate for mitigating most of the ISI, crosstalk (CT), and GN for the windows tested. A canonical filter configuration with two zeros and one pole is shown in Fig. 2.3, where F(z) and X(z) are taken as the z-transforms of F_ζ and X_ζ, respectively. Recall that although the input, output and contents of the N_z delay elements are complex, the multipliers are real. It should probably be emphasized at this point that if the length of each window is less than the intersymbol distance, then the ISI is zero and no digital filters are necessary, since their primary function is to remove ISI. There will be ISI if either window spans more than one symbol.

At this point it is helpful to write a more explicit expression for F_ζ using Eqs. (2.1) - (2.5) and Fig. 2.1:

---

* It is assumed that E_b/N_o and L_t are both expressed in dB.

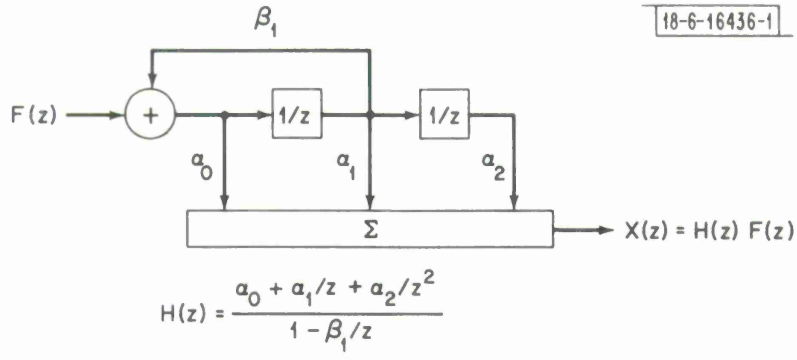

Fig. 2.3. Canonical 2-zero, 1-pole linear digital filter.

$$F_\zeta(k_u) = \sum_n W_N^{(k_u+d_u)n} s(n)\ (w(n+n_u)$$

$$+ \sum_i A_i W_N^{(k_i+d_i)(n_i-n-n_u)} \sum_r x_{i,\zeta+r}\, t(n+n_u-n_i-rN_c)). \tag{2.16}$$

The various components of Eq. (2.16) will now be isolated. As mentioned before, in addition to the signal there are three types of noise excluding LOS interference — interuser noise, intersymbol interference and channel noise. The signal is that part of Eq. (2.16) which is due solely to the ζ-th input symbol from user u:

$$f_{SIG} = A_u \phi_{st}(0) x_{u\zeta}. \tag{2.17}$$

The channel interference (GN) results from the processed channel noise w(n):

$$f_{GN} = \sum_n w(n+n_u) s(n) W_N^{(k_u+d_u)n}. \tag{2.18}$$

The intersymbol interference is due to the other $x_{u\zeta}$:

$$f_{ISI} = A_u \sum_{r\neq 0} x_{u,\zeta+r} \phi_{st}(r). \tag{2.19}$$

The interuser noise is due to everything else:

$$f_{CT} = \sum_{i\neq u} A_i \sum_r x_{i,\zeta+r} \sum_n s(n)\ t(n+n_u-n_i-rN_c) \tag{2.20}$$

$$\cdot\ W_N^{(k_u+d_u)n + (k_i+d_i)(n_i-n-n_u)}.$$

Thus, $F_\zeta(k_u) = f_{SIG} + f_{GN} + f_{ISI} + f_{CT}$ for the ζ-th symbol interval of user u.

From Eqs. (2.17) - (2.20) one may calculate the following autocorrelation functions for the signal and noise terms:

$$R_{SIG}(\zeta - \zeta') = (A_u \phi_{st}(0))^2 \, \delta_{\zeta\zeta'} = R_{SIG}(0) \, \delta_{\zeta\zeta'} \tag{2.21}$$

under the assumption that $R_{xx}(\zeta - \zeta') = \delta_{\zeta\zeta'} = \begin{cases} 1, & \zeta = \zeta' \\ 0, & \text{otherwise} \end{cases}$,

$$R_{GN}(\ell) = N_o \phi_{ss}(-\ell) = N_o \phi_{ss}(\ell) \quad , \tag{2.22}$$

$$R_{ISI}(\ell) = A_u^2 \sum_{\substack{r \neq 0 \\ r \neq -\ell}} \phi_{st}(r) \phi_{st}(r + \ell) \quad , \tag{2.23}$$

and

$$R_{CT}(\ell) = \sum_{i \neq u} A_i^2 \sum_r \sum_{n,m} s(n) \, s(m) \, t(n + n_u - n_i - rN_c)$$

$$\cdot \, t(m + n_u - n_i - (r + \ell)N_c) \, W_N^{(k_u + d_u - k_i - d_i)(n - m + \ell N_c)} \tag{2.24}$$

assuming statistically identical but independent users.

In contrast to the results Eqs. (2.21) - (2.23), $R_{CT}(\ell)$ is complex in general. Sufficient conditions for a real $R_{CT}(\ell)$ are equiamplitude users symmetrically spaced in frequency with respect to user u, i.e., the k_i's are symmetric about k_u modulo N, with zero delays and Doppler shifts. These conditions are not unreasonable at least on the average and therefore the filter is designed to these conditions. A real $R_{CT}(\ell)$ in the design simplifies both the solution of the nonlinear Eq. (2.14) and the resulting filter by permitting half the number of real coefficients $\{\alpha_i, \beta_i\}$. This follows from Eqs. (2.12)

and (2.14) and the fact that

$$R_{FF}(\ell) = R_{SIG}(\ell) + R_{GN}(\ell) + R_{ISI}(\ell) + R_{CT}(\ell) \quad . \tag{2.25}$$

In this report the digital filter is non-adaptive because the $\{\alpha_i, \beta_i\}$ coefficients do not change with time.

A couple of issues involving the recursive filter that have been considered in some detail will be mentioned only briefly in the remainder of this section.

The first issue has to do with prefiltering at the transmitters for reducing ISI. So far the MMSE digital filters have been located in the satellite, i.e., at the output of each user demodulation channel. Conceivably, these compensating filters could instead be placed at the input of each user terminal. The design problem for this input filter option is very similar to that just presented for the output filters, although the equations are slightly different from Eq. (2.13).

After working out the necessary details for an input filter design, one is convinced of the feasibility of the approach but reluctant to program the scheme for computer simulation. The potential gains from an input filter simulation do not seem to justify such an investigation at present. Furthermore, constant envelope signaling at the transmitter is impossible with the input filter.

The second issue has to do with estimating the irreducible error probability due to crosstalk and ISI. The signal-to-noise ratio (SNR) for the overall system can be expressed in terms of the autocorrelation functions of the various signal and noise components and the transfer function of the MMSE filter.

Since the symbol error probability, P_s, in the presence of AWGN can be calculated from the SNR, the theoretical P_s for a typical simulation was estimated using just the SNR. Unfortunately, this estimate was quite pessimistic because the noise is neither white nor Gaussian and because delays and Doppler shifts can corrupt the overall system performance. As a consequence extensive simulation appears to be necessary to establish an accurate performance floor for large SNR's.

2.3.2 The Viterbi Algorithm Approach

The optimal but more complex maximum likelihood decoding approach to the ISI problem is now considered.

When the transmitter and satellite windows are identical, the basic system configuration of Fig. 2.1 conveniently fits the Forney model [48] for the mitigation of ISI using the Viterbi algorithm (VA). In order to greatly simplify the model it is assumed that the interuser interference can be treated as AWGN. Simulation results indicate that this assumption is not a bad one particularly since windows can be selected to make crosstalk (CT) negligible.

From Eqs. (2.17) - (2.19) the received symbol sequence at the output of the DFT of Fig. 2.1 can be written as

$$f(r) = f_{SIG}(r) + f_{ISI}(r) + f_{GN}(r) = Ax(r) \otimes \phi_{ts}(r) + f_{GN}(r) \qquad (2.26)$$

where $\otimes$ represents discrete convolution. In the z-transform domain Eq. (2.26) becomes

$$F(z) = F_{SIG}(z) + F_{ISI}(z) + F_{GN}(z) = AX(z)\ \Phi_{ts}(z) + F_{GN}(z) \quad . \qquad (2.27)$$

The Gaussian noise $f_{GN}(r)$ has the autocorrelation function $N_o\ \phi_{ss}(r)$ from

Eq. (2.22), and the power spectrum $N_o \Phi_{ss}(z)$. Since ϕ_{ss} is an autocorrelation function its z-transform can be factored as

$$\Phi_{ss}(z) = P(z)\ P(1/z) \tag{2.28}$$

where all the zeros of P(z) are inside the unit disc of the z-plane. Since ϕ_{ss} is a sequence of length $2\nu - 1$, P(z) has $\nu - 1$ zeros and is the z-transform of a sequence of length ν, p(r). In the case that the transmitter and satellite windows are identical, t(n) = s(n) and Eq. (2.27) can be rewritten as

$$F(z) = AX(z)\ P(z)\ P(1/z) + N(z)\ P(1/z) \tag{2.29a}$$

$$W(z) = AX(z)\ P(z) + N(z) \tag{2.29b}$$

where n(r) is an AWGN sequence. Equation (2.29b) was obtained from Eq. (2.29a) by division by P(1/z). In terms of an implementation w(r) is the output of a digital filter with impulse response $p^{-1}(r)$ when f(r) is the input. Since the noise component of Eq. (2.29b) is white this filter will be referred to as a whitening filter.

The next step is to attempt the removal of the ISI factor P(z) in Eq. (2.29b) and thereby obtain the input symbol sequence with the transform X(z). The VA performs a maximal likelihood estimation of the entire input sequence in AWGN and is quite well suited to combatting ISI. With this scheme the output digital filter and decision rule of Fig. 2.1 is replaced by the whitening filter and the VA.

The question of the necessary degree $\nu - 1$ of the P polynomials is considered next. Simulations suggest that matched transmitter and satellite windows that extend over more than two symbols may not be required except when the

interfering users are very strong and/or very closely packed in frequency relative to the satellite user being demodulated. For the more reasonable parameter values of the simulation, the additional CT protection was not deemed worth the increase in ISI and, in the case of the peak-power limitation, the signal energy penalty with respect to AWGN. Because of this and the fact that there is no ISI unless the windows span more than one symbol interval, a specific instance of the VA is described and simulated only for the case $\nu = 2$. Although the VA implementation would become more complex, there are no problems with extending the method to larger values of ν.

For $\nu = 2$, Eq. (2.28) has the form

$$\Phi_{ss}(z) = a/z + b + az = (c/z + d)\ (cz + d) \tag{2.30}$$

where $a = \phi_{ss}(1) = \phi_{ss}(-1)$, $b = \phi_{ss}(0)$ and $P(z)$ is the monomial in $1/z$. The whitening filter has the form shown in Fig. 2.4a. In the absence of noise $n(r)$ the output $W(z)$ of the whitening filter of Fig. 2.4a equals the output of the feedforward filter of Fig. 2.4b with input $AX(z)$ and response $P(z)$.

In the VA all possible outputs $\{y(r)\}$

$$y(r) = d \cdot x(r) + cx(r - 1) \tag{2.31}$$

of the noiseless feedforward filter of Fig. 2.4b at a given symbol time r are computed for all possible current input symbols $\{x(r)\}$ and all possible immediately preceding input symbols $\{x(r - 1)\}$. These computations need only be done once, so the answers could be precomputed and stored in a read-only memory (ROM). A subsequence of these $\{y(r)\}$ is then compared to the actual received sequence $z(r)$ out of the whitening filter in such a way as to decide,

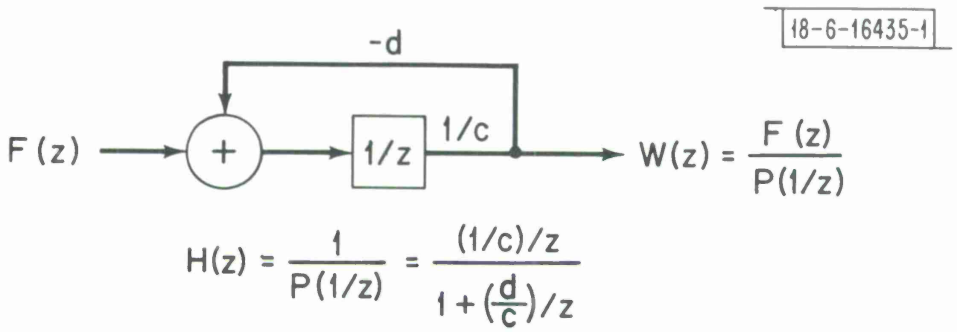

a.

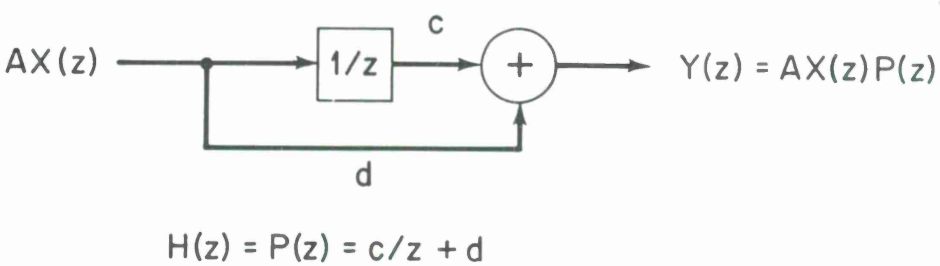

b.

Fig. 2.4. Whitening filter (a) and Viterbi algorithm feedforward filter (b).

with some fixed symbol delay, on the most likely input sequence x(r). Naturally, the most likely input sequence would produce the y(r) subsequence that is closest to the received sequence z(r) in an Euclidean distance sense.

The VA is usually described [49] in terms of a trellis diagram and a set of state sequence paths of finite length L as depicted in Fig. 2.5 for M = 4. For each symbol time r there are $M^{\nu-1}$ possible states or nodes in the r-th column of the trellis, one node for each of the possible input symbols {x(r)}. Let $G_i(r)$ be a real number associated with the node in column r corresponding to the input symbol $x_i(r)$. For the first value of r, $G_i(r) = 0$ for each value of i. Let i' be the row index for the nodes in column $r - 1$. Assume that there are M surviving paths of length L, where the head of each path is a distinct node in column $r - 1$ and where the tail node of each path is a (not necessarily distinct)node in column $r - L$. The likelihood of the path headed by the symbol $x_{i'}(r - 1)$ is measured by the number $G_{i'}(r - 1)$. The first step of the VA is to determine the latest transition to column r for each path in a new set of M surviving paths as follows. The tail nodes of the current set of surviving paths are deleted. Then for each i the M transition numbers $\{g_{i'i}\}$

$$g_{i'i} = |z(r) - (d \cdot x_i(r) + cx_{i'}(r - 1))|^2 \qquad (2.32)$$

are computed using Eq. (2.31), one $g_{i'i}$ for each possible transition from a node in column $r - 1$. The closer the computed $y(r) = d \cdot x_i(r) + cx_{i'}(r - 1)$ is to the received z(r), the smaller the $g_{i'i}$. The latest transition for the new surviving path headed by node ir is determined by an index i' satisfying $G_{i'}(r) = G_i(r)$, where

$$G_i(r) = \min_{i'} (G_{i'}(r - 1) + g_{i'i}) \quad . \qquad (2.33)$$

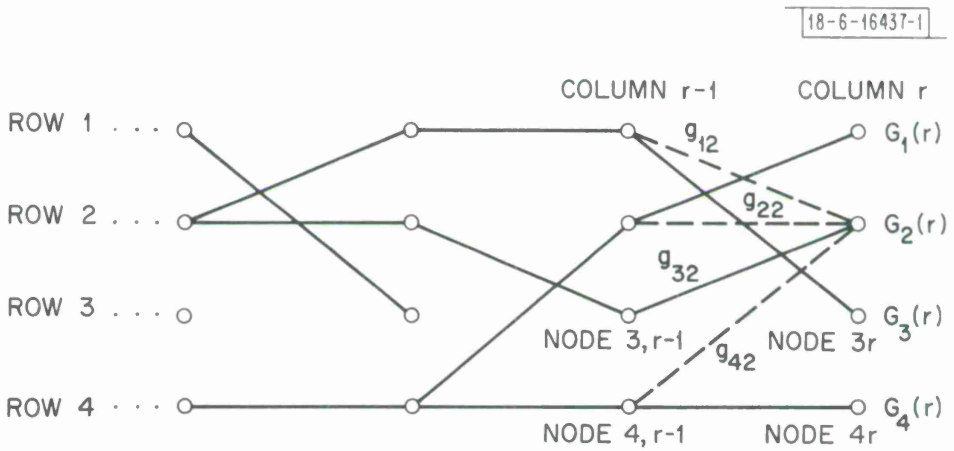

Fig. 2.5. Decoding trellis for Viterbi algorithm.

The other M-1 transitions to node ir are discarded as indicated by the dashed lines to node 2r in Fig. 2.5. The next step of the VA is to output the input symbol corresponding to the tail node of the new most likely surviving path. The head of this path is specified by the index i satisfying $G(r) = G_i(r)$, where

$$G(r) = \min_i G_i(r) \quad . \tag{2.34}$$

The decoded symbol is associated with the node in column r-L-1 belonging to the most likely path. Thus, there is a symbol delay of L-1 due to decoding.

In general, the complexity of the VA varies as M^ν where M is the number of possible input symbol values and ν is the length of the impulse response of the feedforward filter with transform P(z). No multiplications are required during the operation of the VA to obtain the y(r)'s, for a generalization of Eq. (2.31) can be precomputed and stored in a memory of size M^ν 2q-bit words, where 2q is the number of bits required to store a complex number. M^ν complex subtractions, $2M^\nu$ real multiplications and M^ν real additions are required per symbol interval to compute the $\{g_{i',i}\}$, however, cf. Eq. (2.32). Another $M^{2(\nu-1)}$ real additions and $M^{\nu-1}$ $(M^{\nu-1})$-way comparisons are required to compute the real numbers $\{G_i(r)\}$ assigned to the heads of the new paths, cf. Eq. (2.33), and one $(M^{\nu-1})$-way comparison is needed for Eq. (2.34). Furthermore, assuming that M is a power of two, $LM^{\nu-1}$ $(\nu-1)\log_2 M$-bit words of memory are required to store the state sequence paths of length L.

The total costs of the VA with complex arithmetic are indicated in Table 2.1. As already mentioned ν=2 is the primary value of interest. For quadriphase shift keyed (QPSK) modulation, a principal candidate for the communications system at hand, the x(r) symbol alphabet is $\left\{\frac{\pm 1 \pm j}{\sqrt{2}}\right\}$, so M=4. A path

TABLE 2.1

COMPLEXITY OF THE VITERBI ALGORITHM

Operation	Number of Operations per Symbol
real q-bit multiplications	$2M^{\nu}$
real q-bit additions	$M^{2(\nu-1)} + 3M^{\nu}$
real $(M^{\nu-1})$-way comparisons	$M^{\nu-1} + 1$
Memory	
M^{ν} 2q-bit words	
$LM^{\nu-1}$ $(\nu-1)$ $\log_2 M$-bit words	

length L of 10 to 20 is typical for good performance. A q of 5 is usually adequate, though a 4 or 8 bit quantization is more convenient; a word length that is a multiple of four bits is preferable for ease of implemention. For these parameter values, then, the VA requires 32 real multiplications, 64 real additions and 5 4-ary comparisons per symbol. A ROM of 16 8-or 16-bit words and a random-access memory (RAM) of 4 20-to 40-bit words is required.

In comparing the complexity of the VA and MMSE approaches to the ISI problem, the whitening filter of ν-1 delay elements, cf. Fig. 2.4a, must be included in the cost of the VA approach, of course. Considering the fact that a typical MMSE linear recursive filter, cf. Fig. 2.3, requires 8 real multiplications and 6 real additions per symbol, and a RAM of only 3 8-or 16-bit words, it is obvious that the VA approach is much more complex than the MMSE approach. In the computer simulations the performance of these two schemes

was quite comparable (see Section IV).

2.4 Mathematical Model for an MSK Digital System

As stated at the beginning of Section II, minimum shift keying (MSK) is not treated with as much generality as MPSK in this report. In particular, no special windowing is applied at the transmitters with MSK and the satellite windows are restricted to those which introduce no ISI. Under these conditions there is no need for a compensating digital filter or a Viterbi algorithm approach for reducing ISI. These restrictions on the windows have yielded promising simulated results, nevertheless, because of the relatively small crosstalk (CT) between unsynchronized and unwindowed MSK waveforms [8].

Figure 2.6 depicts a digital equivalent model for an MSK system with much the same notation as used in Fig. 2.1 for an MPSK system. In the MSK case two sequences of ± 1 input symbols to user u, $x_{uc\zeta}$ and $x_{us\zeta}$, are converted into a sequence $y_u(n)$ of complex numbers

$$y_u(n) = x_{uc\zeta} \cos \frac{\pi n}{2N_c} + j\, x_{us\zeta} \sin \frac{\pi n}{2N_c} \tag{2.35}$$

where $2N_c$ is the intersymbol distance in each input sequence. The values of $x_{uc\zeta}$ are permitted to change only when $n \equiv N_c$ (modulo $2N_c$), while the values of $x_{us\zeta}$ may change only when $n \equiv 0$ (modulo $2N_c$).

Although the expressions for $z_u(n)$ and $f_{u\zeta}(n)$ given by Eqs. (2.1) and (2.2) still apply, MSK is demodulated differently than MPSK. Referring to Fig. 2.6, the outputs $F_{c\zeta}(k_u)$ and $F_{s\zeta}(k_u)$ are computed from

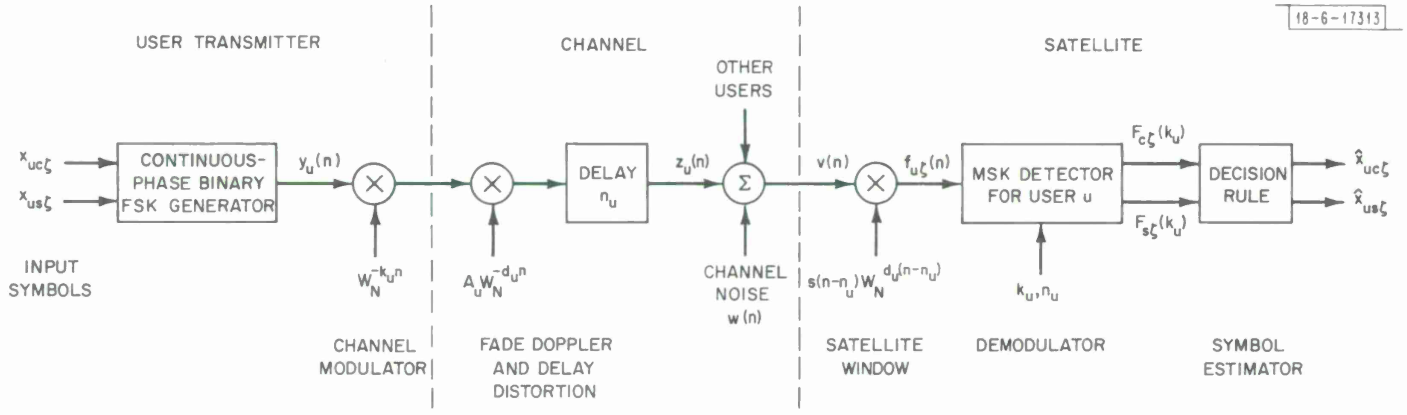

Fig. 2.6. MSK digital system model (only one user path is shown).

$$F_{c\zeta}(k_u) = \sum_{n=-N_c}^{N_c-1} f_{u\zeta}(n + n_u)\, W_N^{nk_u} \cos \frac{\pi n}{2N_c} \tag{2.36a}$$

$$F_{s\zeta}(k_u) = \sum_{n=0}^{2N_c-1} f_{u\zeta}(n + n_u)\, W_N^{nk_u} \sin \frac{\pi n}{2N_c} \tag{2.36b}$$

where the range of the summation index for $F_{c\zeta}(k_u)$ and $F_{s\zeta}(k_u)$ corresponds to the interval when $x_{uc\zeta}$ and $x_{us\zeta}$ must be constant, respectively. Symbol estimates are formed as

$$\hat{x}_{uc\zeta} = \begin{cases} +1, \text{ if } \mathrm{Re}\{F_{c\zeta}(k_u)\} > 0 \\ -1, \text{ otherwise} \end{cases} \tag{2.37a}$$

$$\hat{x}_{us\zeta} = \begin{cases} +1, \text{ if } \mathrm{Im}\{F_{s\zeta}(k_u)\} > 0 \\ -1, \text{ otherwise} \end{cases} . \tag{2.37b}$$

The various components of Eq. (2.36b) for the sine demodulation channel will now be isolated. A similar exercise could be performed for the cosine demodulation channel. Using Eqs. (2.1) and (2.2) and excluding LOS users in Fig. 2.6, the sine channel signal due solely to the ζ-th sine input symbol $x_{us\zeta}$ from user u is

$$f_{sSIG} = x_{us\zeta}\, A_u \sum_{n=0}^{2N_c-1} s(n) \left(\sin \frac{\pi n}{2N_c}\right)^2 . \tag{2.38}$$

The satellite window s(n) is limited implicitly to the intersymbol distance $2N_c$ for MSK, so there is no ISI. The sine channel interference due to the noise w(n) is

$$f_{sGN} = \mathrm{Im}\left\{ \sum_{n=0}^{2N_c-1} w(n + n_u)\, s(n) \left(\sin \frac{\pi n}{2N_c}\right) W_N^{(k_u+d_u)n} \right\} \tag{2.39}$$

and the sine channel crosstalk is given by

$$f_{sCT} = \mathrm{Im}\left\{\sum_{i\neq u} A_i \sum_{n=0}^{2N_c-1} s(n)\left(\sin\frac{\pi n}{2N_c}\right) W_N^{(k_u+d_u)n+(k_i+d_i)(n_i-n-n_u)}\right\} \quad (2.40)$$

cf. Eqs. (2.18) and (2.20), respectively.

III. WINDOWS

The use of data windows for bandwidth conservation in an FDMA mode is the central theme of the approach taken in this report. This section is devoted to the choice and design of the data windows chosen for the system environment outlined in Section I.

3.1 System Aspects

For purposes of exposition and for the bulk of the simulations, an information rate of 16 kbps was assumed. It was further assumed that PSK modulation would be used, that the center frequencies of adjacent channels would be 25 kHz apart and that a maximum contiguous uplink bandwidth of approximately 500 kHz is available for satellite users. Thus up to 20 users can be accommodated. A rate 1/2 convolutional code for greater reliability and QPSK modulation are presumed, although the following discussion also applies to an uncoded BPSK system. In either case the channel symbol rate is 16000 symbols/sec which corresponds to an intersymbol spacing T_c of 62.5 μsec. Recognizing that narrowband LOS users may also have frequency allocations in the uplink bandwidth, the worst case situation of 20 LOS users spaced by 25 kHz and interspersed between 20 satellite users is presumed. The problem is thus to design data windows to control both the interuser and LOS interference with respect to any satellite user.

A discrete window sequence is used to achieve spectral shaping, both to minimize interference between adjacent satellite users and to reduce interference from LOS users operating at nearby frequencies. In the worst case the LOS users will be operating on 25 kHz centers and the satellite users will also be forced to operate on 25 kHz centers in the cracks between LOS channels as

shown in Fig. 3.1. Clearly, the available center frequency to cutoff bandwidth for a given satellite user must not exceed 12.5 kHz. In order to see what effect the choice of a transmitter window t(n) has upon the shape of the signal spectrum, the signal at the output of one particular user transmitter is analyzed.

Let $\xi_u(n)$ represent the discrete sequence formed by the application of the transmitter window. $\xi_u(n)$ can then be written, cf. Fig. 2.2 and Eq. (2.5), as

$$\xi_u(n) = \sum_{r=R_0}^{R_1} x_{ur} \exp\left[j \frac{2\pi}{N} k_u n\right] t(n - rN_c) \quad . \tag{3.1}$$

Here R_0 and R_1 are used to denote indices of the first and last symbols transmitted, respectively, and N is a parameter which controls (along with k_u) the center frequency of the satellite user. If the window t(n) is of finite length (the only case considered), then only a few of the terms in Eq. (3.1) contribute to the sum for a given value of n. The Fourier transform of this signal can be written as

$$\begin{aligned} \Xi_u(e^{j\omega}) &= \sum_{n=-\infty}^{\infty} \xi_u(n) e^{-j\omega n} \\ &= \sum_{n=-\infty}^{\infty} \sum_{r=R_0}^{R_1} x_{ur} \exp\left[j \frac{2\pi}{N} k_u n\right] t(n - rN_c) \exp[-j\omega n] \\ &= T\left(\exp\left[j\left(\omega - \frac{2\pi k_u}{N}\right)\right]\right) \sum_{r=R_0}^{R_1} x_{ur} \exp\left[-jrN_c\left(\omega - \frac{2\pi k_u}{N}\right)\right] \end{aligned} \tag{3.2}$$

where $T(e^{j\omega})$ is the Fourier transform of t(n). The power density spectrum of

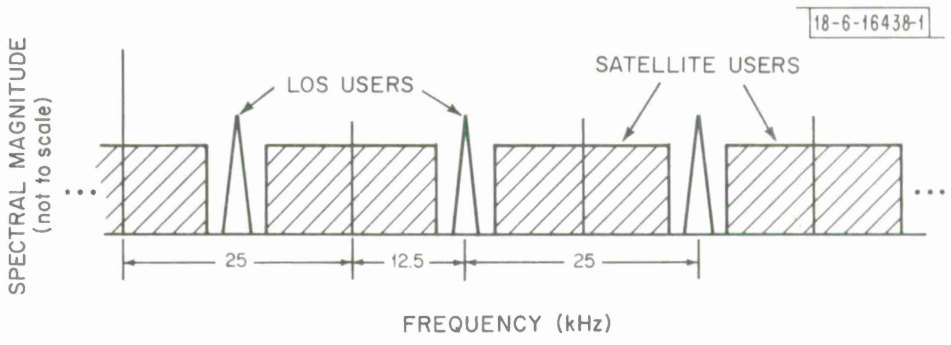

Fig. 3.1. Worst case frequency allocations.

this signal can be expressed as

$$\overline{|\Xi(e^{j\omega})|^2} = |T\left(\exp\left[j\left(\omega - \frac{2\pi k_u}{N}\right)\right]\right)|^2 \qquad (3.3)$$

assuming that the information symbols are uncorrelated.

The D/A converter of Fig. 1.1 is clocked with an intersample time of $T_s = T_c/N_c$. Thus, if $\tilde{\Xi}(j\Omega)$ denotes the transform of the continuous (analog) output of the D/A converter, then from the sampling theorem

$$\tilde{\Xi}(j\Omega) = T_s \, \Xi(e^{j\Omega T_s}) \qquad (3.4a)$$

and

$$\overline{|\tilde{\Xi}(j\Omega)|^2} = T_s^2 \, |T\left[\exp j\left(\Omega T_s - \frac{2\pi k_u}{N}\right)\right]|^2 \quad . \qquad (3.4b)$$

This is an important result for it identifies the shape of the signal spectrum with the Fourier transform of the transmitter window. In particular the power spectral density of the u-th user is the magnitude of the Fourier transform of the window squared and displaced in frequency by k_u/NT_s. Thus, to locate satellite users at odd multiples of 12.5 kHz we require $1/N = 12.5 \times 10^3 \, T_s$. Since $T_s = T_c/N_c$ with $T_c = 62.5$ μsec, this implies that

$$N_c = \frac{25N}{32} \quad .$$

For the number of samples per symbol N_c to be an integer, N should thus be a multiple of 32. N represents the total number of satellite channels available, but only half of these channels can have center frequencies which are located at odd multiples of 12.5 kHz. In order to have at least 20 usable 16 kbps channels and to permit a simple FFT realization in the satellite, N was chosen to be the least power of two larger than 32, i.e., 64. This fixes the number of samples per symbol N_c at 50 and yields a total analysis bandwidth of 800 kHz

which represents the basic clock rate for the A/D and D/A converters. A similar analysis could be carried out for different data rate channels.

Two different classes of windows were selected for study — the Dolph-Chebyshev windows and the prolate spheroidal windows. For a given length and cutoff frequency each of these windows is optimum in some sense — a Dolph-Chebyshev window has a minimum equiripple response outside of the main lobe of its frequency response and a prolate spheroidal window has minimum energy out of band. Each of these windows has an adjustable parameter so that its bandwidth can be controlled, and each has a real, even frequency response which aids in the implementation of the system. Since the prolate spheroidal window was both easy to work with and also optimal in a particularly useful way, other windows were not used extensively. It is extremely doubtful that another window can be found that will improve the performance of the system measurably. These two window families will be discussed in the following two sections. Since a given window could be applied at either the transmitter or the satellite, the generic notation w(n) for the data window and $W(e^{j\omega})$ for its Fourier transform will be used just in these sections.

3.2 The Dolph-Chebyshev (DC) Window

The DC window represents the optimal equiripple window. A DC window of length N_w with cutoff frequency ω_c has a digital frequency response

$$W(e^{j\omega}) = \frac{\cos(N_w \cos^{-1}(z_o \cos(\omega/2)))}{\cosh(N_w \cosh^{-1} z_o)} \tag{3.5a}$$

$$z_o = \frac{1}{\cos(\omega_c/2)} \tag{3.5b}$$

as shown in Fig. 3.2. For a given sidelobe height δ, the DC window has the

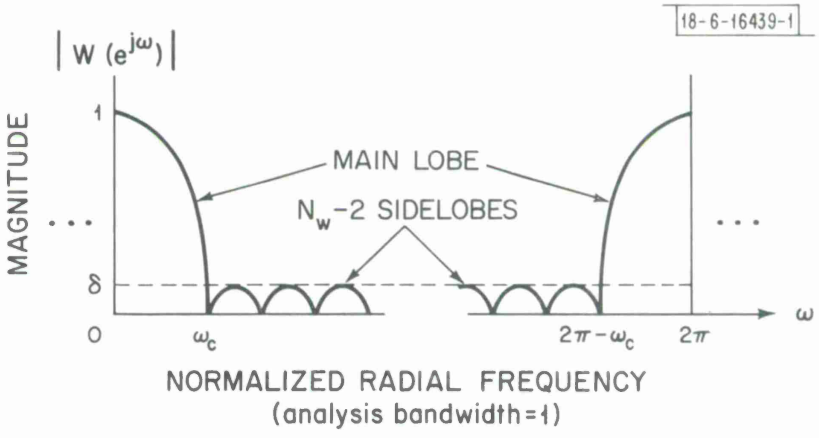

Fig. 3.2. Dolph-Chebyshev spectral window.

smallest mainlobe width ω_c of any window of the same order. Alternatively, for a given mainlobe width the DC window has the smallest maximum sidelobe height. All of the sidelobes are of the same height, so the window is called equiripple. This implies that to a given user all other equal power users contribute the same amount of interference whether they are located on an adjacent channel or separated by several channels. The total crosstalk energy received from other users is thus directly proportional to the number of such users.

For a communication channel with a center frequency to cutoff bandwidth of $f_c = \omega_c/2\pi$ Hz and an intersample time T_s, according to Helms [50] the sidelobe ripple δ is bounded by

$$\log_{10} \frac{2}{\delta} \lesssim \frac{f_c T_s N_w}{0.73} \quad . \tag{3.6}$$

Using T_s = 1.25 μsec for a given f_c, one can compute the tradeoff between the window length and the peak sidelobe ripple. This information is displayed graphically in Fig. 3.3.

In order to adequately reduce interference among different users for the signal strengths expected, and system parameters described above, more than 20 dB of rejection will be required. Consequently, DC windows will have to be more than 50 samples (one symbol length) long as seen from Fig. 3.3. This will result in intersymbol interference which will have to be mitigated by post filtering in the satellite.

Several Dolph-Chebyshev data windows and their frequency responses were computed and utilized in the simulations. It was noted that short windows possess a large spike in their time-domain. This is a possibly severe drawback if short windows were to be used with peak-power-limited transmitters for

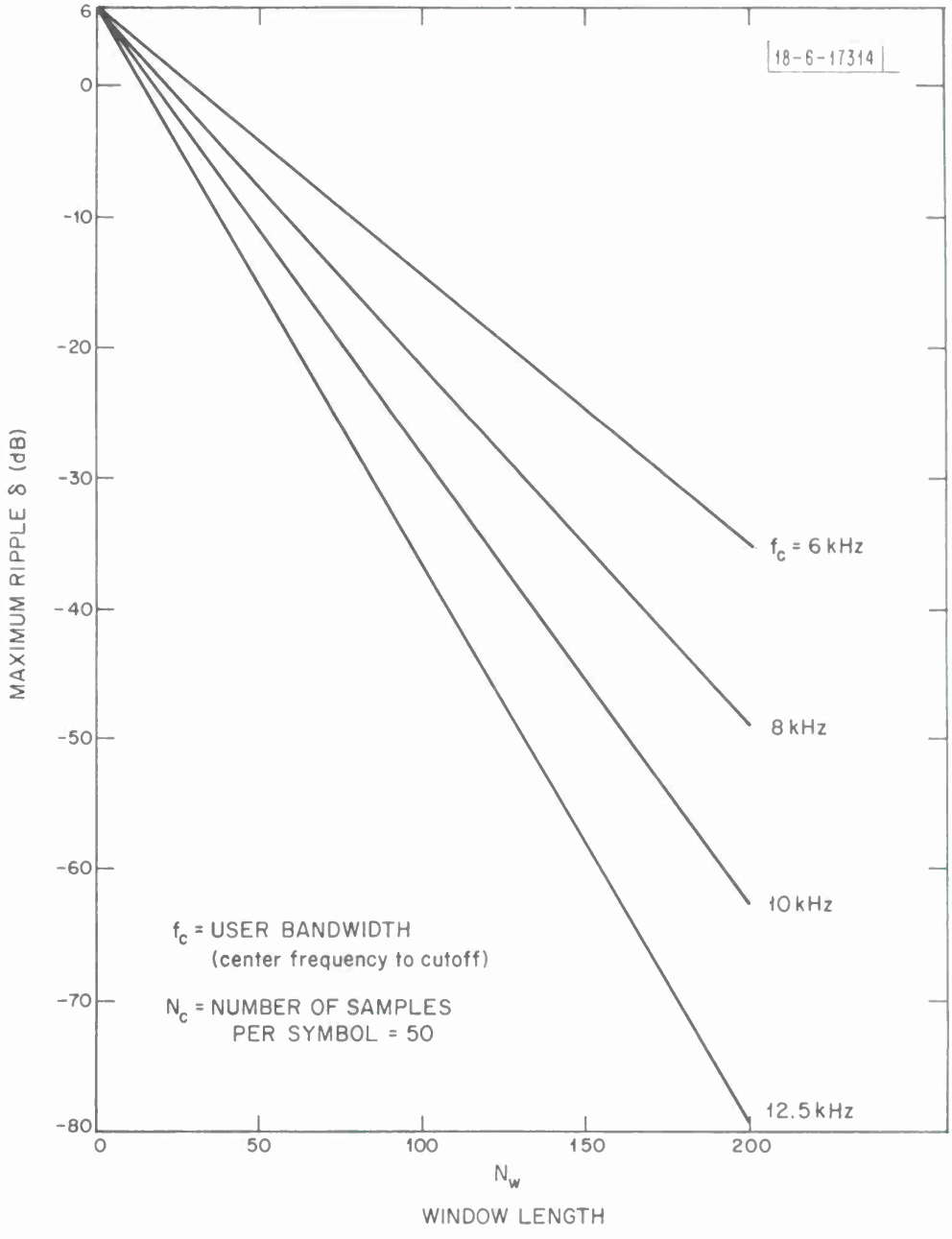

Fig. 3.3. Sidelobe level vs window length for Dolph-Chebyshev window and analysis bandwidth of 800 kHz.

it limits the average power which can be transmitted.

Each data window was computed by periodically sampling the frequency response of Eq. (3.5a) and then computing the inverse discrete Fourier transform (DFT)

$$w(n) = \frac{1}{N_w} \sum_{k=0}^{N_w-1} W\left(e^{j\frac{2\pi k}{N_w}}\right) e^{j\frac{2\pi kn}{N_w}}, \quad n = 0, 1, \ldots, N_w - 1 \quad . \quad (3.7)$$

The data windows were normalized for a peak-power-limited transmitter. In particular they were normalized so that the energy in a rectangular window of length N_w is unity, cf. Eqs. (2.8) - (2.10). A non-rectangular window represents an energy loss L_t due to the peak-power-limitation at the transmitter. In those cases where there is no peak-power-limitation, this energy loss does not appear.

The sampled crosscorrelation functions $\phi_{st}(\ell)$

$$\phi_{st}(\ell) = \sum_{m=0}^{\nu N_c-1} s(m)\, t(m - \ell N_c)$$

for some of the computed DC data windows are displayed in Fig. 3.4. The center pulse ($\ell = 0$) from each set represents the fraction of the signal energy which remains after the two windowing operations. The height of the pulses on the sides represents the amount of intersymbol interference (ISI) which is present. Only when both windows span only one symbol is no ISI introduced. Figure 3.4a depicts the case with windowing at both the transmitter and the satellite. Here $s(n) = t(n) = w(n)$ using Eqs. (3.5) and (3.7). Figure 3.4b and c depict DC windowing only at the satellite with a rectangular shaped data window at the transmitter. In Fig. 3.4a and b the transmitter and satellite windows

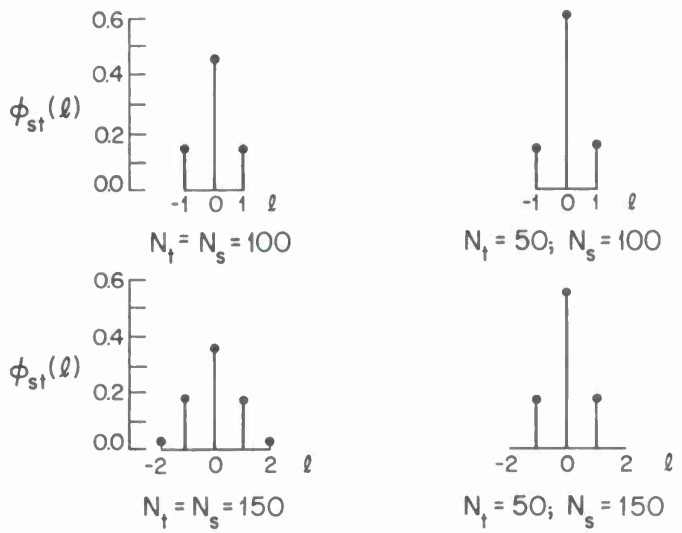

a. Matched.

b. Constant envelope. [centered t(n)]

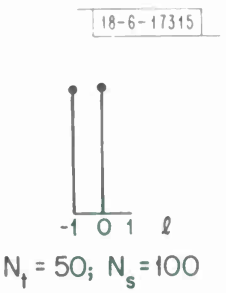

c. Constant envelope. [t(n) right of center]

Fig. 3.4. Crosscorrelation functions for Dolph-Chebyshev windows (transmitter window t(n) of length N_t and satellite window of length N_s).

are aligned when $\ell = 0$, i.e., they have a common vertical centerline. In Fig. 3.4c the non-zero portion of the transmitter window is shifted one symbol interval to the right. The cases represented in Fig. 3.4b and Fig. 3.4c permit constant envelope signaling at the transmitter, because t(n) is rectangular and one symbol in length, while allowing the option of centering the non-zero part of a satellite window of length $N_c < N_s \leq 2N_c$ over a 3 or 2 symbol interval, respectively.

3.3 The Prolate Spheroidal (PS) Window

The prolate spheroidal windows represent optimal windows in the sense that of all windows with length N_w they have the smallest amount of energy outside the band $(-\omega_c, \omega_c)$. For this reason they are superior to the Dolph-Chebyshev (DC) family in many cases. They are a little more difficult to generate, however. Their generation will be more completely understood if the form of the window is derived from basic considerations.

Consider any window w(n) of length N_w with Fourier transform

$$W(e^{j\omega}) = \sum_{n=0}^{N_w-1} w(n)\ e^{-j\omega n} \quad . \tag{3.8}$$

One wishes to find that w(n) for which the energy contained in the frequency band $(-\omega_c, \omega_c)$ is a maximum.

Restated, the problem is to find the w(n) which maximizes

$$\beta^2 = \frac{\int_{-\omega_c}^{\omega_c} |W\ (e^{j\omega})|^2\, d\omega}{\int_{-\pi}^{\pi} |W\ (e^{j\omega})|^2\, d\omega} \quad . \tag{3.9}$$

This problem is similar to the problem for continuous signals which was solved by Landau and Pollack using prolate spheroidal wave functions [51,52]. The following approach for discrete signals obviously borrows from their earlier work.

From Eq. (3.8) and Parseval's relation

$$\int_{-\pi}^{\pi} \left| W\left(e^{j\omega}\right) \right|^2 d\omega = 2\pi \sum_{n=0}^{N_w-1} |w(n)|^2 \quad . \tag{3.10}$$

Thus, Eq. (3.9) becomes

$$\beta^2 = \frac{\int_{-\omega_c}^{\omega_c} \sum_{n=0}^{N_w-1} w(n)\, e^{-j\omega n} \sum_{m=0}^{N_w-1} w^*(m)\, e^{j\omega m} d\omega}{2\pi \sum_{n=0}^{N_w-1} |w(n)|^2}$$

$$= \frac{\sum_{n=0}^{N_w-1} w(n) \sum_{m=0}^{N_w-1} w^*(m)\, \frac{\sin \omega_c (m-n)}{(m-n)}}{\pi \sum_{n=0}^{N_w-1} |w(n)|^2} \tag{3.11}$$

where $w^*(m)$ is the complex conjugate of $w(m)$. From the Cauchy-Schwartz inequality,

$$\left\{ \sum_{n=0}^{N_w-1} a^2(n) \right\} \left\{ \sum_{n=0}^{N_w-1} b^2(n) \right\} \geq \left\{ \sum_{n=0}^{N_w-1} a(n)\, b(n) \right\}^2 \tag{3.12}$$

with equality if and only if $b(n) = c \cdot a(n)$, where c is any constant. If Eq. (3.12) is applied to Eq. (3.11) with

$$a(n) = w(n) \tag{3.13a}$$

$$b(n) = \frac{1}{\pi} \sum_{m=0}^{N_w-1} w^*(m) \frac{\sin \omega_c (m-n)}{(m-n)} \tag{3.13b}$$

then the maximum value of β^2 will occur when

$$\lambda_o w(n) = \sum_{m=0}^{N_w-1} w^*(m) \frac{\sin \omega_c (n-m)}{\pi(n-m)} \quad . \tag{3.14}$$

Here λ_o is a constant, and w(m) is real. According to the form of Eq. (3.14) λ_o must thus be an eigenvalue of that equation. The value of β^2 that results is straightforwardly computed as λ_o by substituting Eq. (3.14) into Eq. (3.11). Thus to maximize β^2 one must find the largest eigenvalue of Eq. (3.14) and choose w(n) to be the corresponding eigenfunction.

Some examples of these PS windows obtained by a standard numerical method [53] are shown in Fig. 3.5. The data windows are normalized in the same way as the DC data windows. The energy loss L_t for peak-power-limited transmitters is also shown in Fig. 3.6.

In Fig. 3.7 the fraction of out-of-band energy $1-\lambda_o$ is plotted as a function of N_w for different values of user bandwidth. In contrast to the DC windows the co-channel interference decreases as the channel separation is increased due to the spectral roll-off of the PS windows. Thus, with PS transmitter windows system performance will be less sensitive to interference from equal power users at larger frequency deviations.

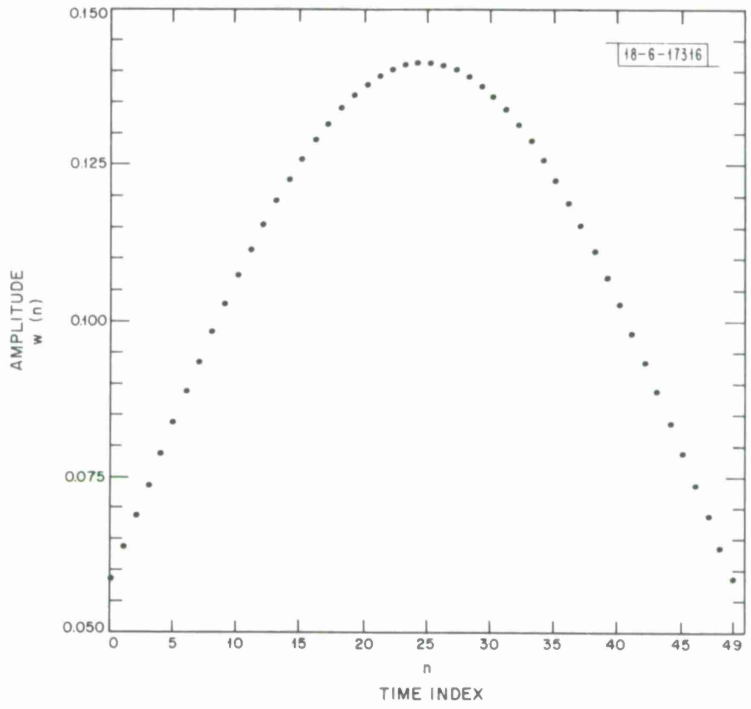

a. 50-point data window.

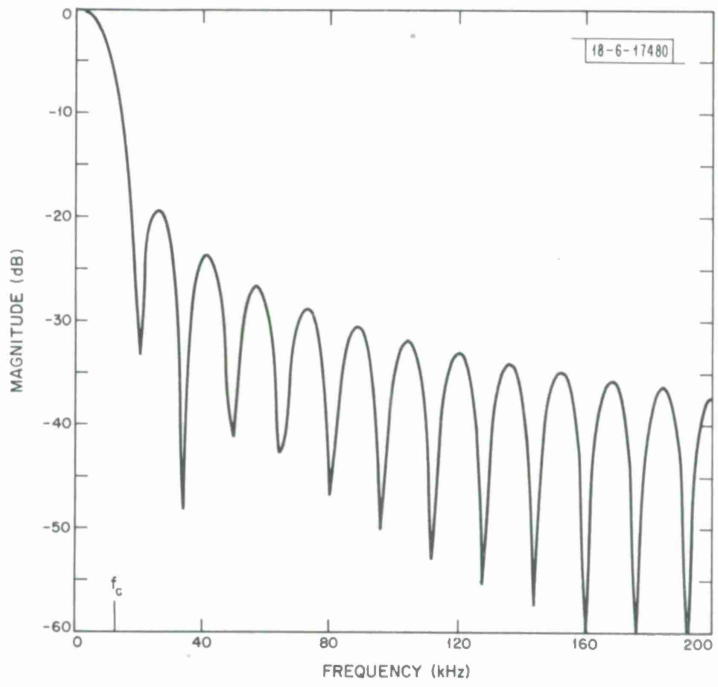

b. 50-point spectral window.

Fig. 3.5. Prolate spheroidal windows for f_c = 12.5 kHz and an analysis bandwidth of 800 kHz.

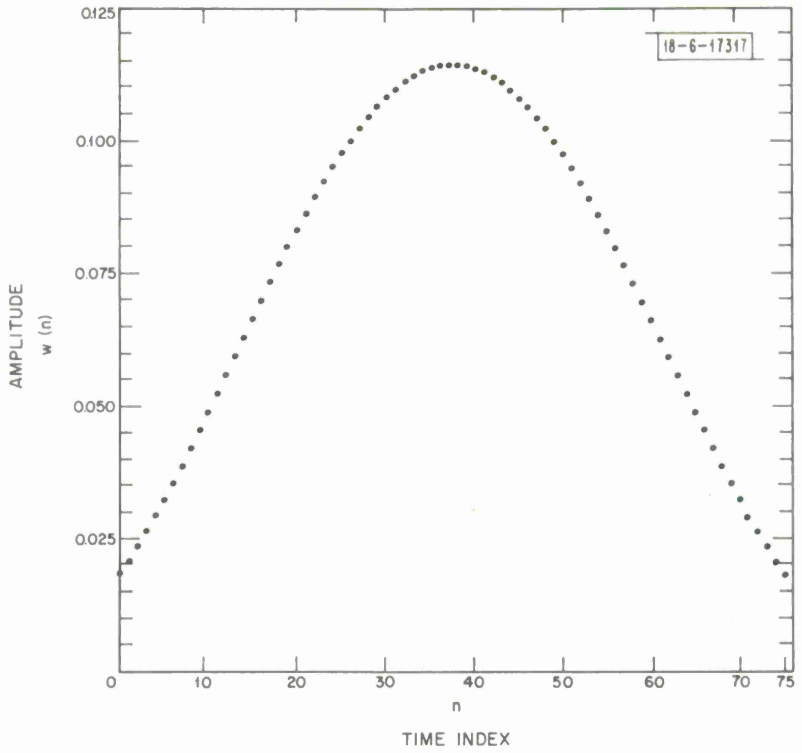

c. 76-point data window.

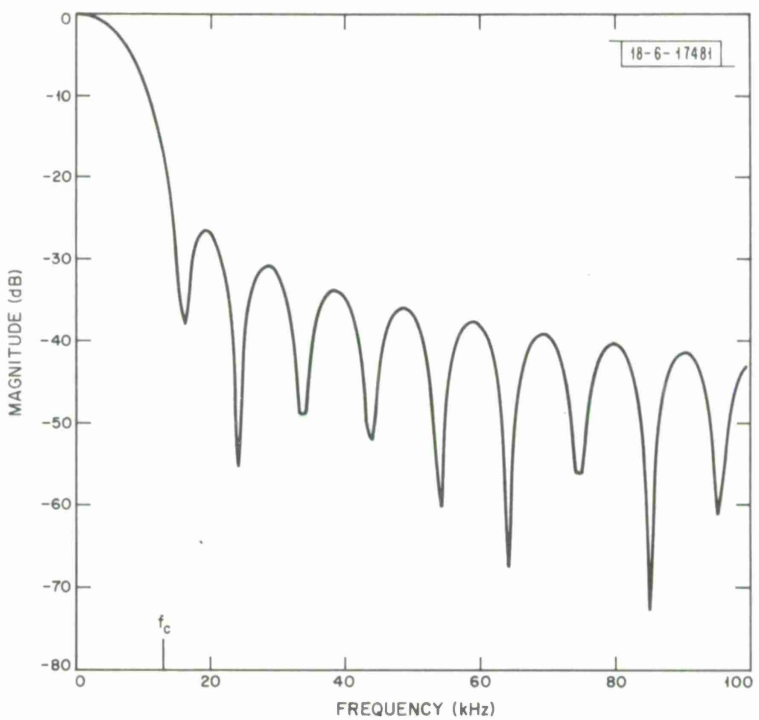

d. 76-point spectral window.

Fig. 3.5 Continued.

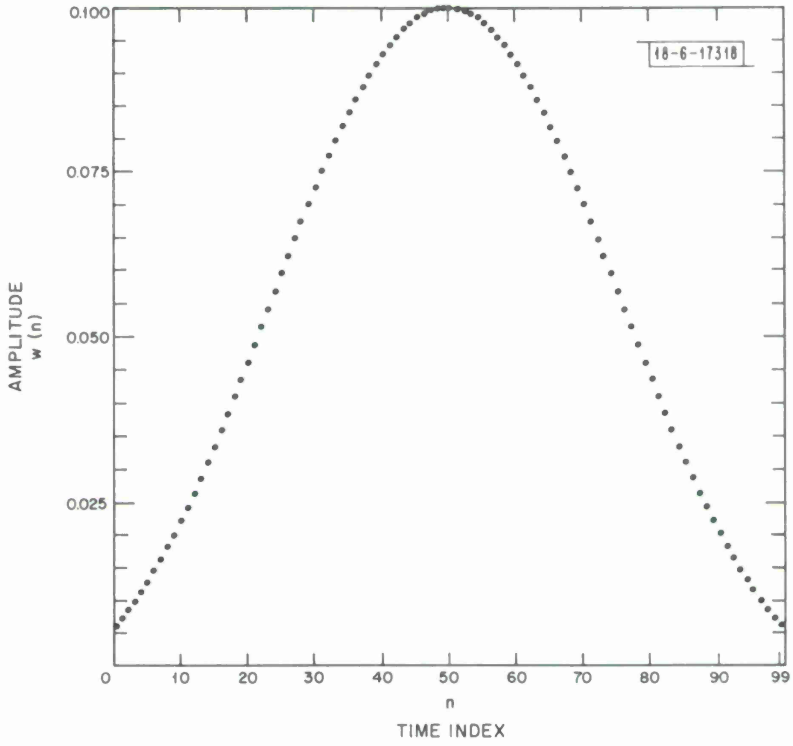

e. 100-point data window.

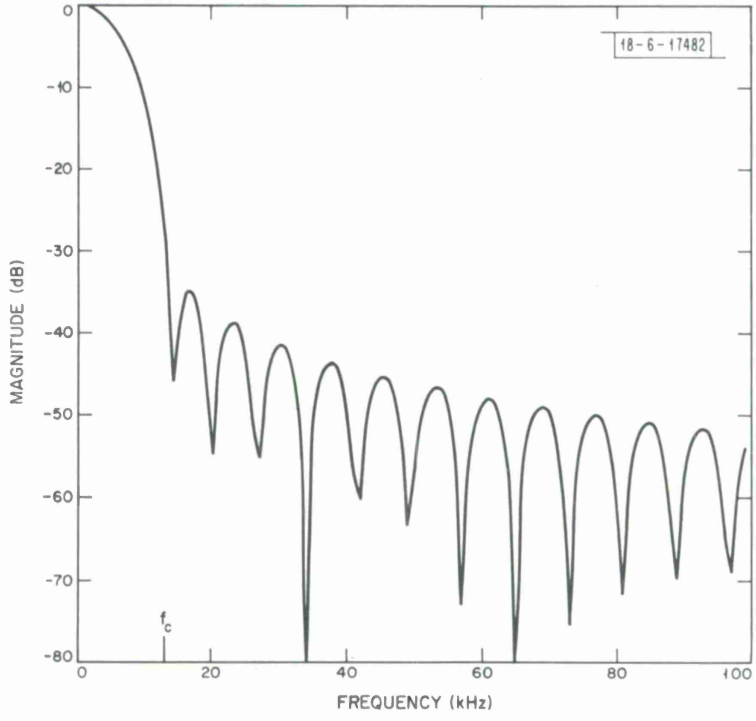

f. 100-point spectral window.

Fig. 3.5 Continued.

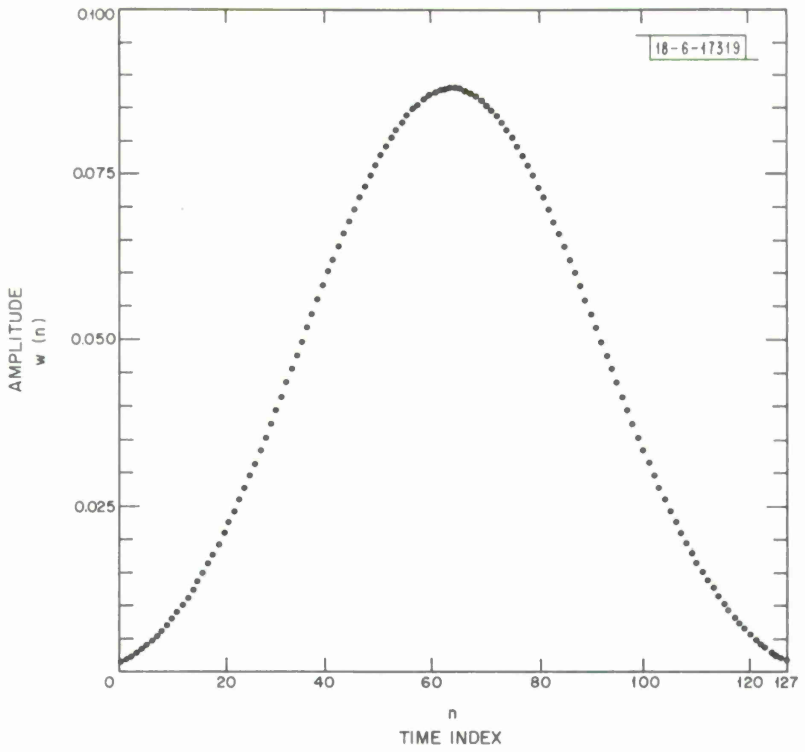

g. 128-point data window.

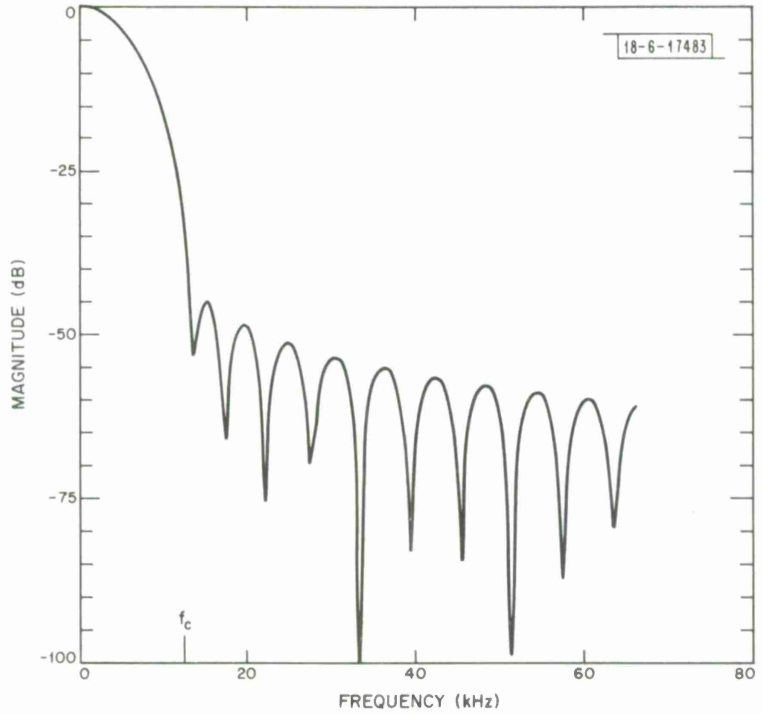

h. 128-point spectral window.

Fig. 3.5 Continued.

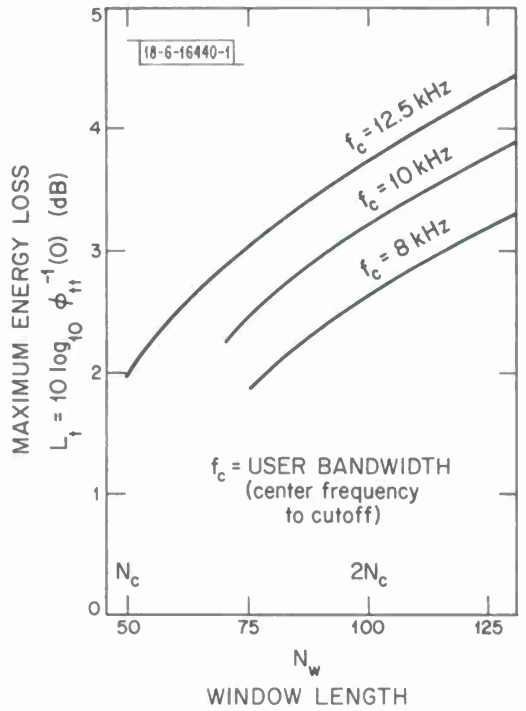

Fig. 3.6. Maximum energy loss for prolate spheroidal windows with peak-power-limited transmitter.

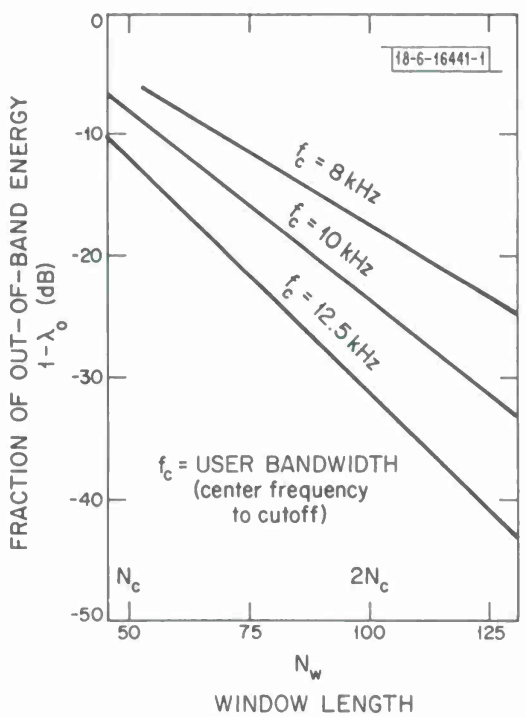

Fig. 3.7. Fraction of out-of-band energy for prolate spheroidal windows.

The crosscorrelations $\phi_{st}(\ell)$ for these PS data windows are displayed in Fig. 3.8. This figure is the prolate spheroidal counterpart to Fig. 3.4.

Detailed descriptions of how these windows performed will be deferred to Section IV, although, as might be expected, the PS windows are to be preferred over the DC windows. The PS windows are more natural for use in conjunction with the MMSE filters of Section 2.3. In addition, the decreasing sidelobe level of the PS family is probably of greater importance than the slightly narrower mainlobe of the DC family. Finally, the spikes in the DC data window can be a disadvantage for peak-power-limited transmitters.

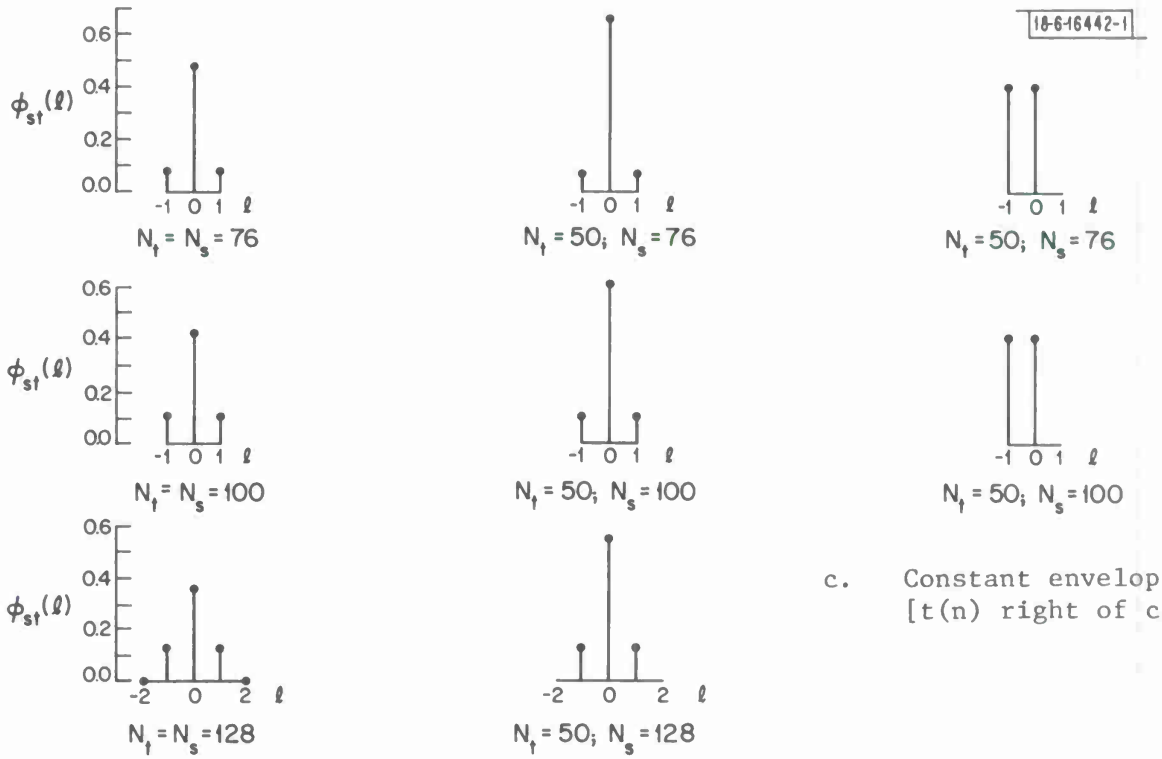

a. Matched.

b. Constant envelope. [centered t(n)]

c. Constant envelope. [t(n) right of center]

Fig. 3.8. Crosscorrelation functions for prolate spheroidal windows (transmitter window t(n) of length N_t and satellite window of length N_s).

IV. PERFORMANCE

In this section selected results from an extensive computer simulation using data windows for bandwidth conservation are presented.

4.1 Rationale of Simulation

Simulation was used to estimate symbol error probabilities since analytic expressions for the error are difficult to obtain in the presence of interuser interference. Even when the windows shape the user spectra sufficiently so that the crosstalk (CT) between users is negligible and computable bounds for the intersymbol interference (ISI) error can be applied, simulation has still proven useful to determine how much ISI can be removed with a simple MMSE filter. Direct simulation has the additional advantage that all signaling schemes can be compared on a common basis.

A flexible set of computer programs has been developed for generating Dolph-Chebyshev (DC) and prolate spheroidal (PS) windows, designing MMSE filters for given transmitter and satellite windows, and performing the indicated simulations for satellite users employing BPSK, QPSK, and CPFSK modulation. The scheme of Forney, cf. Section 2.3.2, which uses the Viterbi algorithm to obtain a maximum likelihood estimate of the transmitted data sequence in the presence of AWGN and ISI has also been programmed. LOS users, when simulated, are modeled as colored Gaussian noise generated by passing AWGN through a narrowband digital filter.

Although many options can be simulated, computer time is expensive. A typical experimental run over 1000 symbols consumes on the order of 1 minute of IBM 370/168 CPU time. Such run lengths are sufficient, however, to permit reasonably tight confidence intervals for the measured error probabilities in

the E_b/N_o range of 2 to 12 dB. The authors have chosen to spend computer time investigating a variety of system options with moderate statistical variances in the resulting data instead of just a few options with longer runs and smaller variances.

4.2 Qualitative Results

Initially LOS users were ignored and data were gather for QPSK satellite users under several different windowing modes. Allowing for the case that some user signals could be as much as 10 dB weaker than others at the receiver, it was quickly established that non-rectangular windows spanning more than one symbol were necessary for a viable level of performance (e.g., a P_s symbol error probability between 10^{-2} and 10^{-3} at an E_b/N_o of 10 dB). Hence, with QPSK users it was not possible to achieve the system objectives without introducing ISI. Next, it was determined that constant envelope (CE) QPSK signaling (rectangular transmitter window spanning one symbol interval) and a long satellite window covering more than one symbol (which introduces ISI) performed rather poorly. The superior CT properties of MSK suggest that CE MSK signaling with either a rectangular or non-rectangular satellite window s(n) may be feasible. In fact simulations indicate that MSK modulation is a very attractive keying scheme for uncoded data. Finally matched PS windows (s(n) = t(n)) yielded promising results for QPSK with window lengths between one and two symbol intervals. In this latter case a simple MMSE digital filter was as effective at removing intersymbol interference as a maximum likelihood estimator based on the Viterbi algorithm. The DC windows proved to be uniformly inferior to the corresponding PS windows.

Although BPSK (binary phase shift keying) users were not simulated

extensively, the existing data and theory suggests that the qualitative observations from the study of QPSK would also apply to BPSK. The major difference is that the BPSK simulation reflects the uncoded situation while the 16000 4-ary symbols per sec rate QPSK allows for a performance improvement via a rate 1/2 convolutional code. (See Section 4.5.)

In the absence of interfering LOS users the windows for the satellite users were somewhat arbitrarily designed to have a cutoff frequency of 12.5 kHz. It was natural to consider a smaller cutoff frequency in dealing with LOS interference. This provides an extra degree of freedom that hopefully would help reduce LOS interference by narrowing the main lobe of the spectral window. For a fixed window length, however, a narrower main lobe means larger sidelobes hence increased CT among users. The simulations showed that the original cutoff frequency of 12.5 kHz was superior even in the presence of the LOS interference modeled, evidently because the sidelobe effects dominated.

Before presenting some quantitative results to illustrate the foregoing conclusions, the format of the simulations will be described.

4.3 Scope of the Simulation

Twenty-one prolate spheroidal and Dolph-Chebyshev windows have been generated for simulation. The window characteristics are summarized in Appendix A. Window lengths between 50 and 200 samples were used spanning between one and four input symbols.

Windows whose lengths were between 64 and 100 samples were simulated in two ways — once with the total span extending over only two symbol intervals, and once with the span extending over parts of three symbol intervals. The centering of a window is not important in the design of a MMSE compensating

filter but the simulations for the two cases were different. Although the simulation evidence is not conclusive, the authors tend to favor using three symbol intervals for these windows.

Simulations were also performed using 50-point windows which due to their one symbol length produce no intersymbol interference. For these windows no correction filters are necessary and the output of the DFT is itself an estimate of the transmitted symbol.

The cutoff frequency for the spectrum of the overall signal was varied between 8 and 12.5 kHz. The windows with lower cutoff frequencies were used in experiments with simulated LOS users. In the bulk of the simulations, however, LOS users were not simulated.

It was always assumed that several users would be transmitting over separate channels simultaneously. Due to a variety of factors (atmospheric conditions, unequal distances from the transmitters to the satellite, etc.) these users will not be received at the satellite with equal energies. It is important nonetheless that the weaker channels still be reliable. Thus, it was generally assumed that all users except the one being demodulated would be received with energy E times that of the user of interest. E varied from 0 to 20 dB. On some runs the E for a given user was taken to be a random variable uniformly distributed between 0.25 and 2.25. Interfering users were either chosen to be synchronized or unsynchronized. In the latter case each user was given a random delay. These delays were uniformly distributed between 0 and 1 symbol interval. They were also given Doppler shifts relative to one another of up to $\pm$ 500 Hz. In all cases the user signal being demodulated is assumed to be synchronized with respect to its own receiver.

The characteristics of the MMSE filters for reducing ISI are listed in Appendix B. The coefficients of these filters depend upon the specific transmitter and satellite windows chosen. Each filter was designed assuming 10 equal energy satellite users, zero delays and Doppler shifts, and a certain level of channel noise.

The satellite user frequencies employed in the filter design and simulation were either closely packed (which represents a worst case crosstalk situation) or loosely spaced. In the packed case adjacent users were placed at frequencies $\pm$ 25 kHz, $\pm$ 50 kHz,... from the user being demodulated. In the spaced case, the frequency spacing was three times as great.

Although all of the digital filters were designed to minimize the mean-square error (MSE) between the actual and desired outputs, the filters could contain any number of poles and zeros. The MSE figure was used to select promising filter configurations. The smaller the MSE, the greater the degree of ISI removed. This figure generally increases with the channel noise and with the window length as shown in Fig. 4.1 for some 2-zero, 1-pole filters designed for matched PS windows. Adding more than one pole (feedback path) to the filter made little significant improvement in either the MSE or in the performance of the system. Adding more than two zeros (three feedforward terms) to the filter reduced the MSE significantly only for windows longer than 100 samples.

4.4 Quantitative Data

The most significant simulation data justifying the qualitative results of Section 4.2 will be presented in this section. In almost all cases each simulated datum was based on 1000 observations.

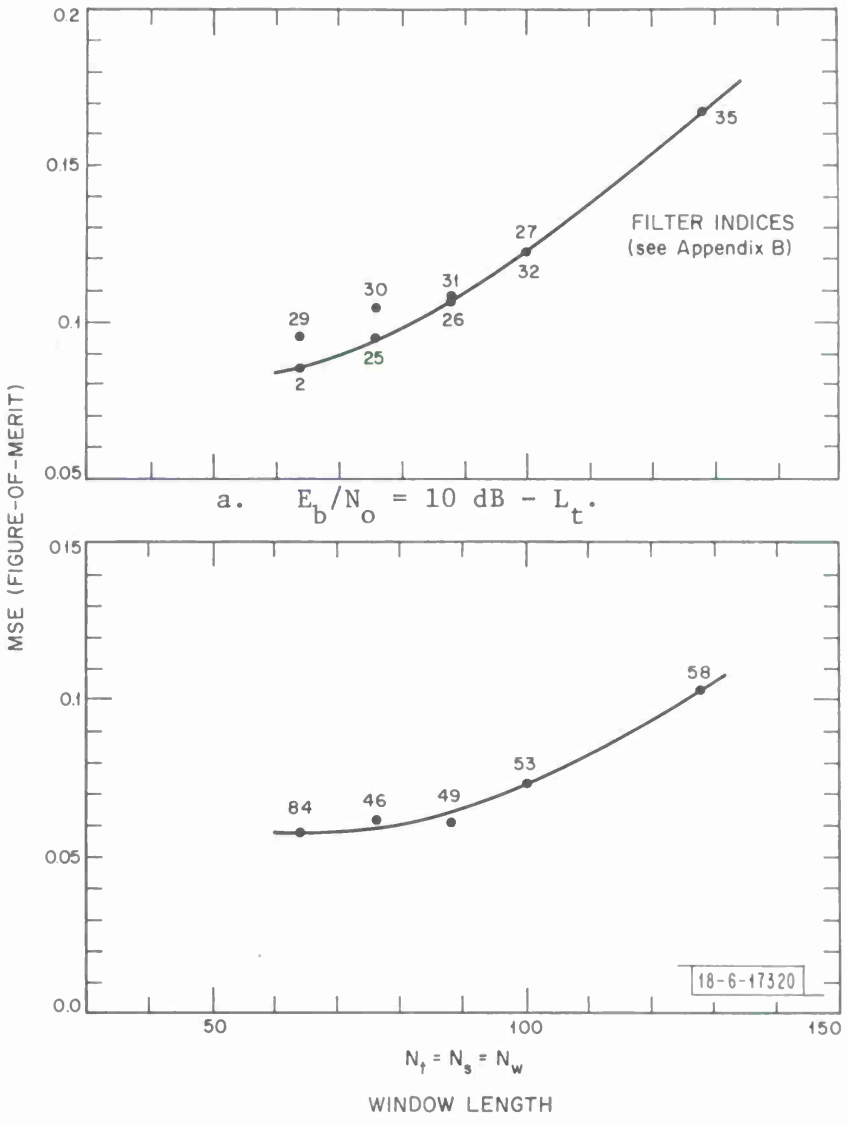

Fig. 4.1. MSE figure-of-merit for filter designs with peak-power-limited transmitter (matched PS windows, f_c = 12.5 kHz, N_z = 2, N_p = N_d = 1).

In Fig. 4.2 the performance of a 50-point prolate spheroidal window at the satellite is shown both with a constant envelope (CE) 50-point rectangular transmitter window and with a 50-point matched PS transmitter window. When the users are all synchronized, the matched window is clearly superior and in the unsynchronized case neither window performs adequately. These data were gathered for 10 dB interfering users (E = 10) and were plotted assuming a strictly peak-power-limited transmitter (loss L_t = 1.96 dB due to transmitter window). The effects of Doppler shifts were unsignificant in this case.

There is an advantage to using a CE transmitter window against channel noise, when the transmitter is peak-power-limited. In Fig. 4.3, therefore, a 50-point CE transmitter window is paired with a 128-point PS satellite window and a 150-point DC satellite window. The other users in this case had random timing asynchronies, but no significant Doppler shifts. The cases of 0 dB, 6 dB and 10 dB interfering users are shown. It will be observed that the PS window is slightly better than the DC in this case and that neither window is adequate in the presence of strong interfering users. These results are supported by other simulations. From these data it can be safely concluded that nearly perfect power control would be required for CE signaling with QPSK. On the other hand there was a clear improvement for unsynchronized users with the longer windows over the case presented in Fig. 4.2.

Neither the one symbol matched window configuration nor the CE transmitter window just discussed will perform adequately if the synchronization and transmitter power control requirements are relaxed. By contrast, for QPSK, matched satellite and transmitter windows which span more than one symbol interval will perform well in this situation as evidenced by the data presented in Fig. 4.4.

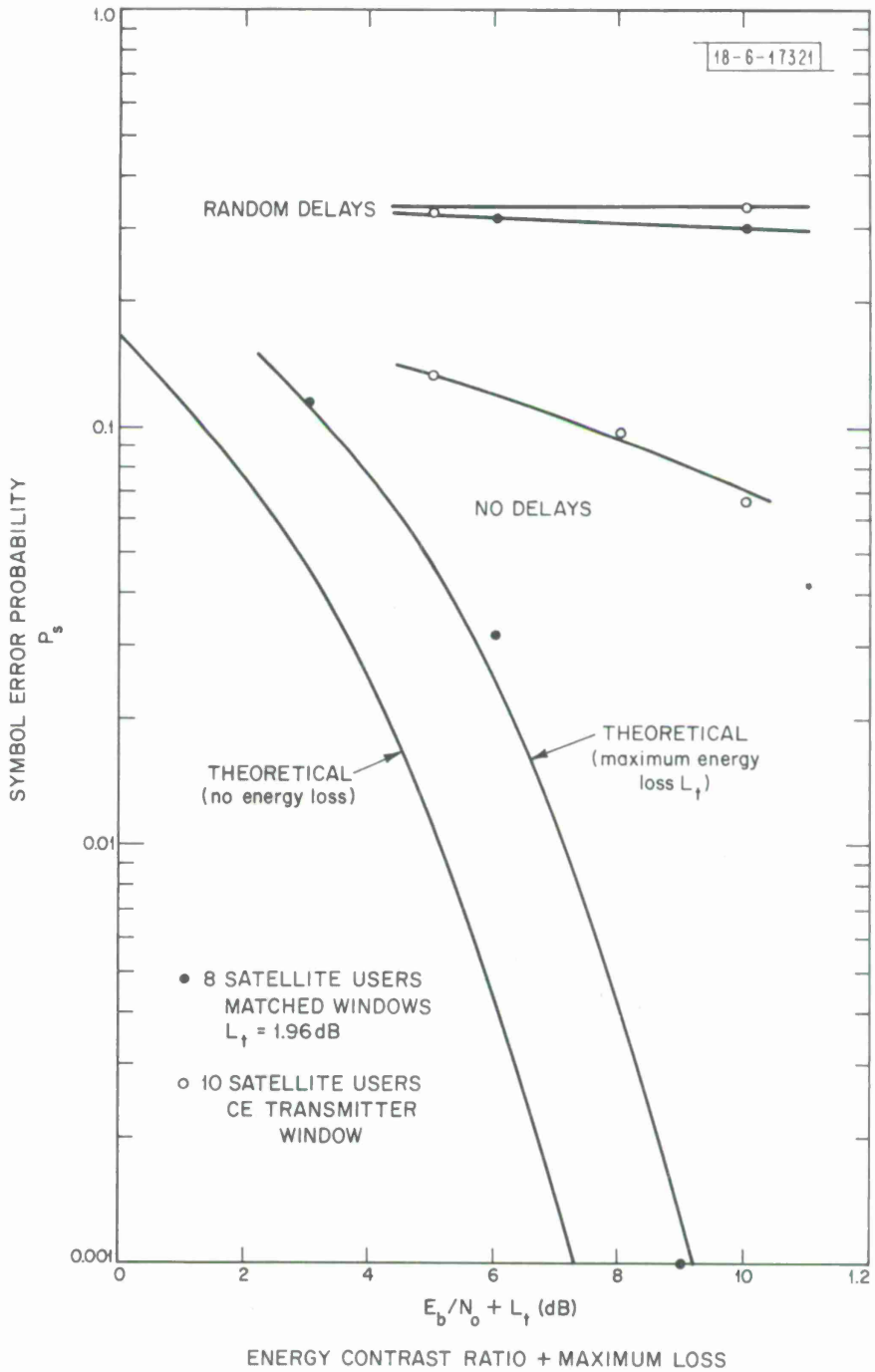

Fig. 4.2. Uncoded 16k symbols/sec QPSK performance for one-symbol prolate spheroidal satellite window.

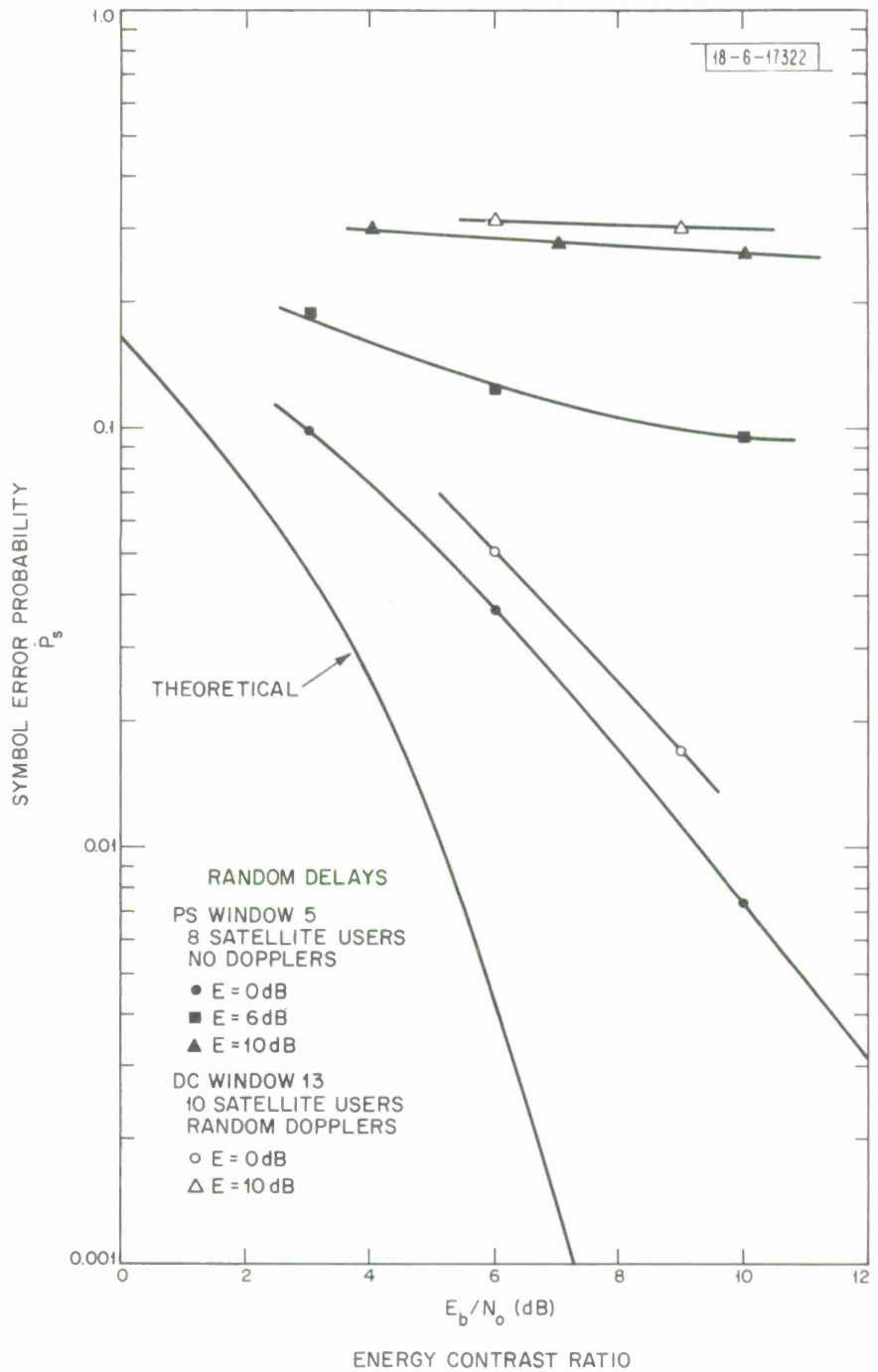

Fig. 4.3. Uncoded 16k symbols/sec QPSK performance for constant envelope transmitter window and long satellite window.

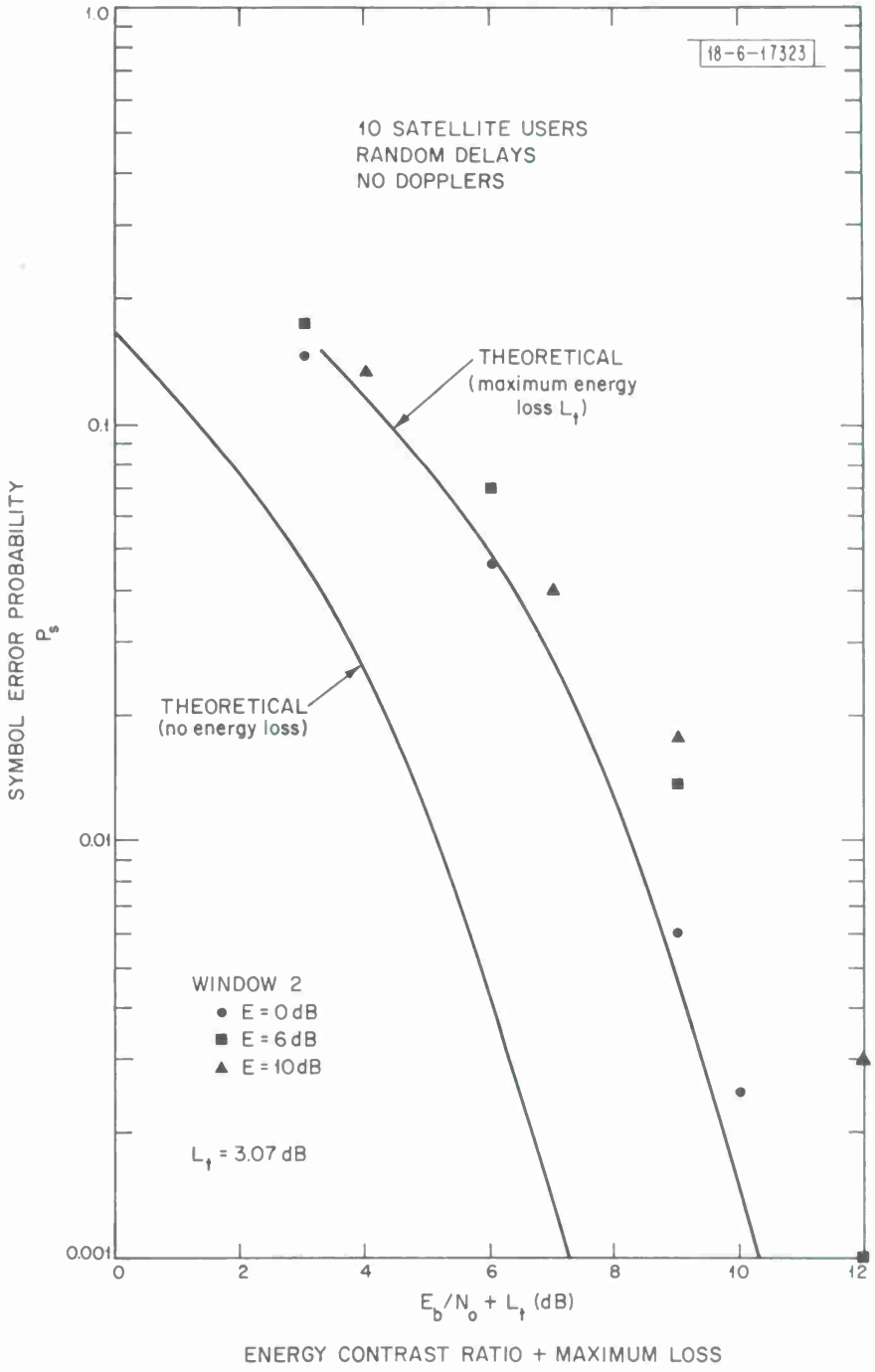

Fig. 4.4. Uncoded 16k symbols/sec QPSK performance for matched prolate spheroidal windows with peak-power-limited transmitters.

For equal amplitude satellite users the data agree very closely with the theoretical QPSK curve reflecting the maximum 3.07 dB energy penalty in the presence of AWGN due to the non-rectangular signal envelope. The compensating MMSE digital filter performs well in reducing the ISI introduced by these relatively short 76-point (about 3/2 symbol intervals) windows. These short windows do a good job in controlling crosstalk since there is only a 0.5 to 2.5 dB degradation from the theoretical curve for interfering users as much as 10 dB stronger than the user being demodulated.

The use of a whitening filter and Viterbi algorithm to remove intersymbol interference yielded eventually the same performance as the MMSE filter for an E_b/N_o up to about 12 dB. The former maximum likelihood approach is to be preferred for higher signal-to-noise ratios.

With longer windows there is increased ISI and an increased penalty to be paid for the shape of the signal envelope. With 200-point matched PS windows the maximum energy penalty is 3.76 dB and there is a 1 dB increase in the residual ISI in the E_b/N_o range of 6 to 12 dB. Thus, in general, as the data windows are made longer the CT is reduced at the price of increased ISI and vulnerability to AGWN under a peak-power constraint at the transmitters.

Figure 4.5 illustrates the consistent observation that matched DC windows are inferior to matched PS windows, especially when the interfering satellite users are strong relative to the user being demodulated. There is also more residual ISI with a DC window than with the corresponding PS window. This discrepancy is particularly severe for long windows. Consequently, Dolph-Chebyshev windows will be eliminated from further consideration.

Up to now only satellite users have been simulated. Next some results

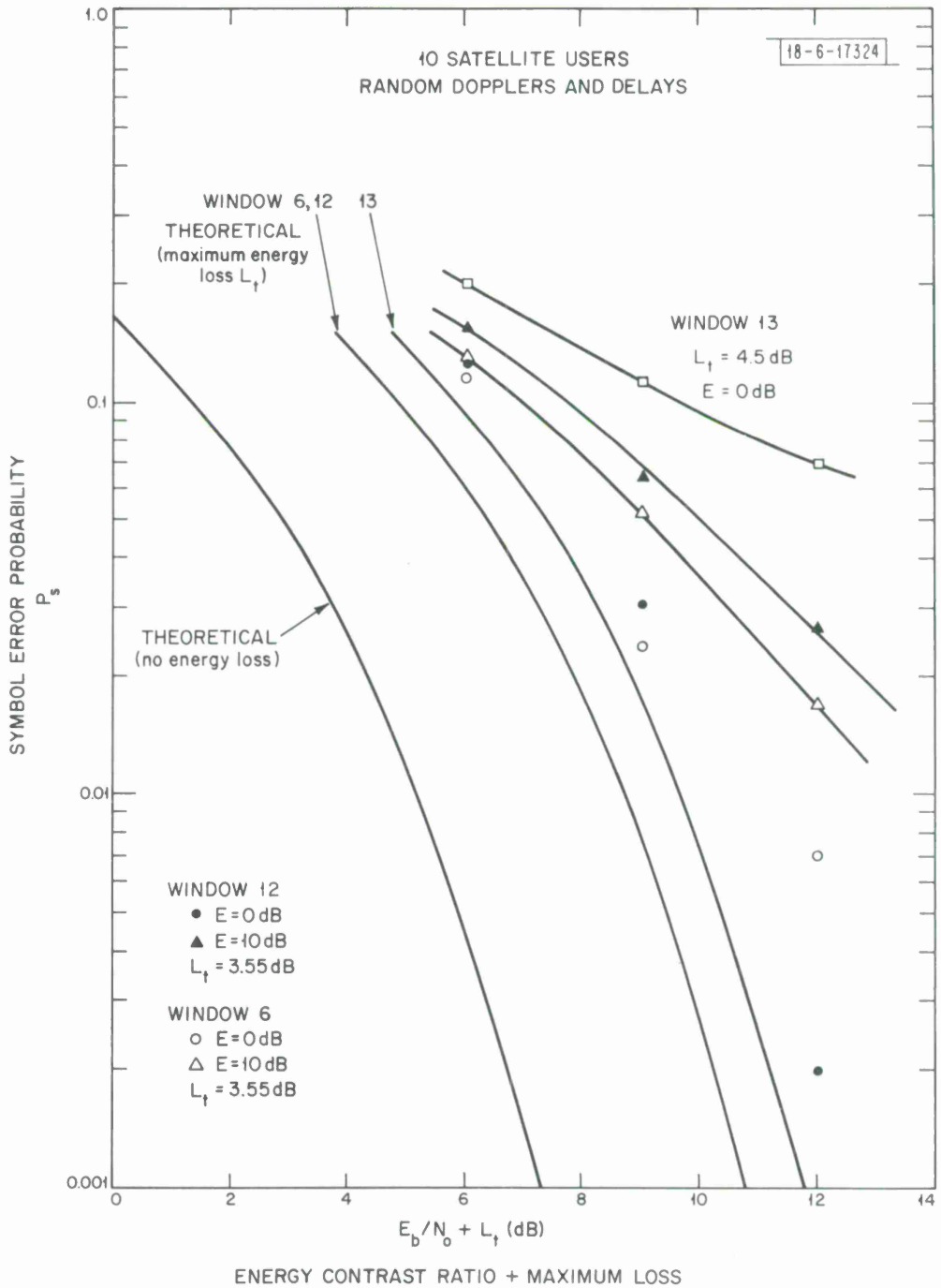

Fig. 4.5. Uncoded 16k symbols/sec QPSK performance for matched Dolph-Chebyshev windows with peak-power-limited transmitters.

obtained with LOS as well as satellite users will be presented.

The designers of the satellite system presumably have no real control over the LOS users but only limited knowledge of the LOS frequency allocations, nominal bandwidth and modulation formats, etc. A typical LOS user* would be of relatively narrow bandwidth and located at a multiple of 25 kHz. Aside from this a given LOS modulation characteristics could be just about anything. Accordingly, the LOS users are modeled simply as narrowband-filtered (colored) Gaussian noise at the appropriate center frequencies. The nominal bandwidth of these users was set in the range 3 to 5 kHz and their pre-filtered mean-square signal amplitude was set about 8 dB and 11 dB above the user of interest for QPSK and MSK, respectively,assuming a rectangular transmitter window. In these simulations two LOS users were assumed located on each side of the user being demodulated as shown in Fig. 4.6. Although more LOS users could be included in this model, the filtering action of the satellite window guarantees that any additional LOS users would have only a secondary effect.

Figure 4.7 presents data for three different pairs of matched windows. Window 2 has a frequency cutoff of 12.5 kHz, window 15 cuts off at 8 kHz and window 18 cuts off at 10 kHz. All three of the PS windows are 76 points long. It should be noted that the 12.5 kHz window performs better despite the fact that it has the largest maximum energy penalty L_t. In comparing Figs. 4.4 and 4.7 it is seen that the presence of these LOS users does not degrade performance significantly for E_b/N_o in the range 4 to 12 dB for this window.

---

* There is a predominance of amplitude modulated voice communication with a 6 kHz bandwidth at UHF.

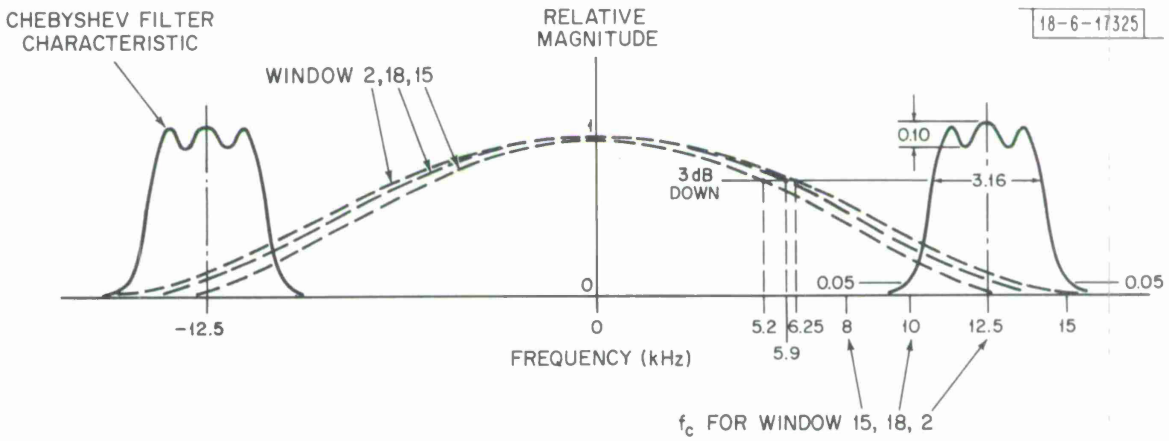

Fig. 4.6. Line-of-sight user model.

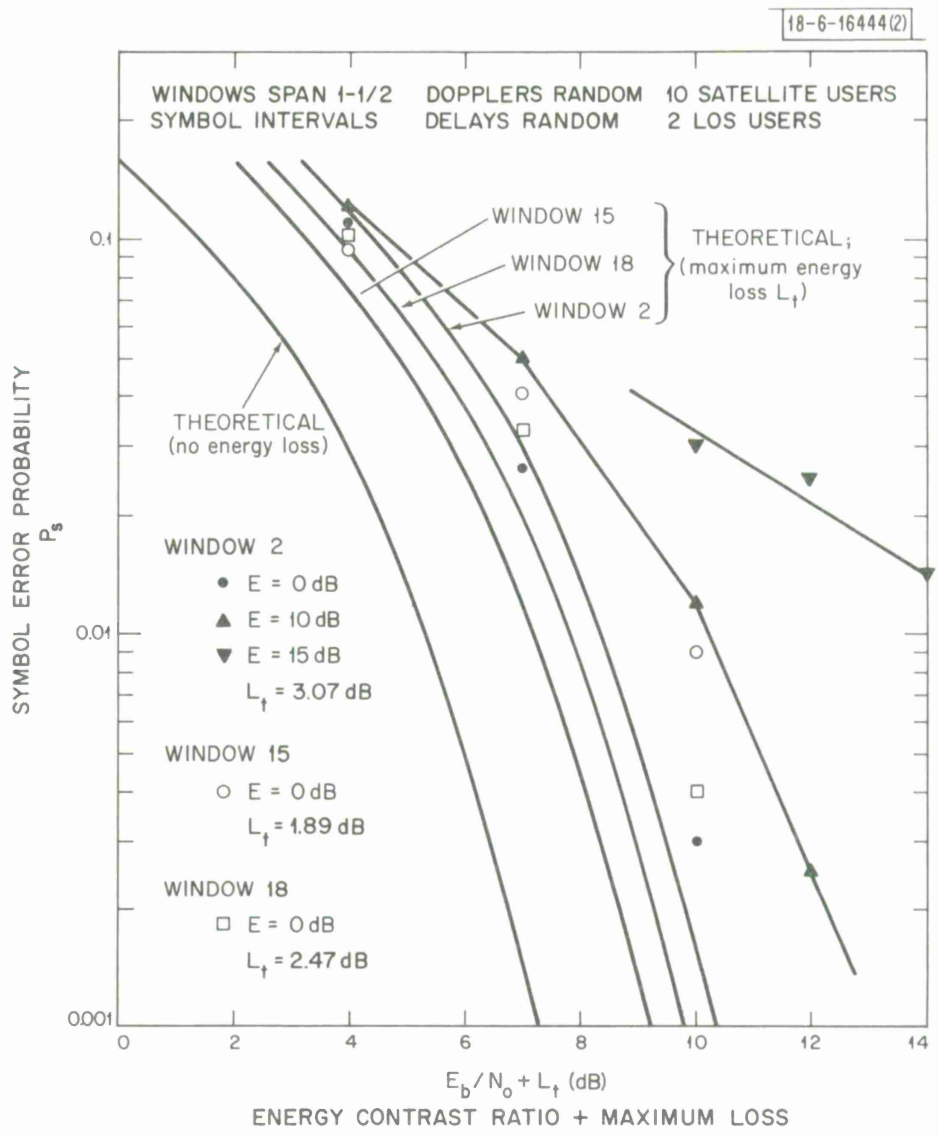

Fig. 4.7. Uncoded 16k symbols/sec QPSK performance for matched prolate spheroidal windows with peak-power-limited transmitters and LOS users.

Thus, PS windows of moderate length are capable of handling both CT and a particular form of LOS interference for the closely packed FDMA situation outlined in Section 3.1. Since the transmitter and satellite windows need not be identical, the designer is free to modify the transmitter and satellite windows individually to tradeoff the different types of interference. Increasing the length and perhaps reducing the cutoff frequency of the satellite window provides added protection against stronger LOS users but at the expense of more ISI. A longer transmitter window would help in reducing CT among satellite users but also would mean more of an AWGN energy loss under a peak-power limitation at the transmitter and more ISI.

Hence, the close frequency packing of equiamplitude, unsynchronized, QPSK 16 kbps satellite users on 25 kHz centers and in between LOS users appears to be possible with only a small loss in performance ($< 1/2$ dB for $P_s \geq 10^{-3}$) compared to the theoretical AWGN case. With no transmitter power control and 10 dB interfering users the price in performance could be as large as 2 or 3 dB above the theoretical for $P_s \geq 10^{-3}$. As explained in Section 4.5 a few dB less E_b/N_o would be possible with the use of the rate 1/2 convolutional code mentioned previously to improve the overall performance [54,55]. The simulated performance for uncoded BPSK satellite users resulted in nearly the same losses as with QPSK before the coding improvement.

Returning to the question of maintaining CE signaling by not using special transmitter windows, simulation data for continuous phase FSK modulation will be presented next. The emphasis will be on MSK rather than CPQFSK since MSK has a greater potential for controlling crosstalk (CT) among satellite users at the closely packed center frequencies assumed. It was verified by simulation

that CPQFSK performance is indeed very poor. If a non-rectangular satellite window is applied to MSK, it is confined to two (binary) symbol intervals to avoid introducing ISI.

The uncoded bit error probability vs E_b/N_o performance for 10 closely packed MSK users at 4800 bps and a center frequency spacing of 3750 Hz is shown in Fig. 4.8. In this case a rate 1/2 convolutional code is assumed so that with coding the information rate is 2400 bps. The code is capable of improving the performance shown by approximately 2 or 3 dB for the equiamplitude user case. Performance is adequate if there is perfect power control of the transmitting users, but it is evident that the CT interference is too severe without a high degree of power control. A satellite window here noticeably degraded performance.

If the user spacing is tripled the precoding performance is very close to the theoretical curve in AWGN even when the interfering users are 10 dB larger than the user being demodulated. Thus, the higher channel symbol rate MSK is not very promising because either a transmitter power control discipline must be imposed on the users or too much bandwidth must be sacrificed which is contrary to the original system objectives. Conceivably a rate 3/4 convolutional code and a 3600 Hz symbol rate would fare better at the 3750 Hz spacings than the 1/2 rate code, but it seems doubtful that coded MSK can beat uncoded MSK at these closely packed frequencies.

Some very encouraging uncoded MSK results are shown in Fig. 4.9. With two LOS users the performance is within 1 dB of the theoretical bit error probability curve even with 10 dB interfering users. The application of a 100-point prolate spheroidal satellite window has little effect for interfering

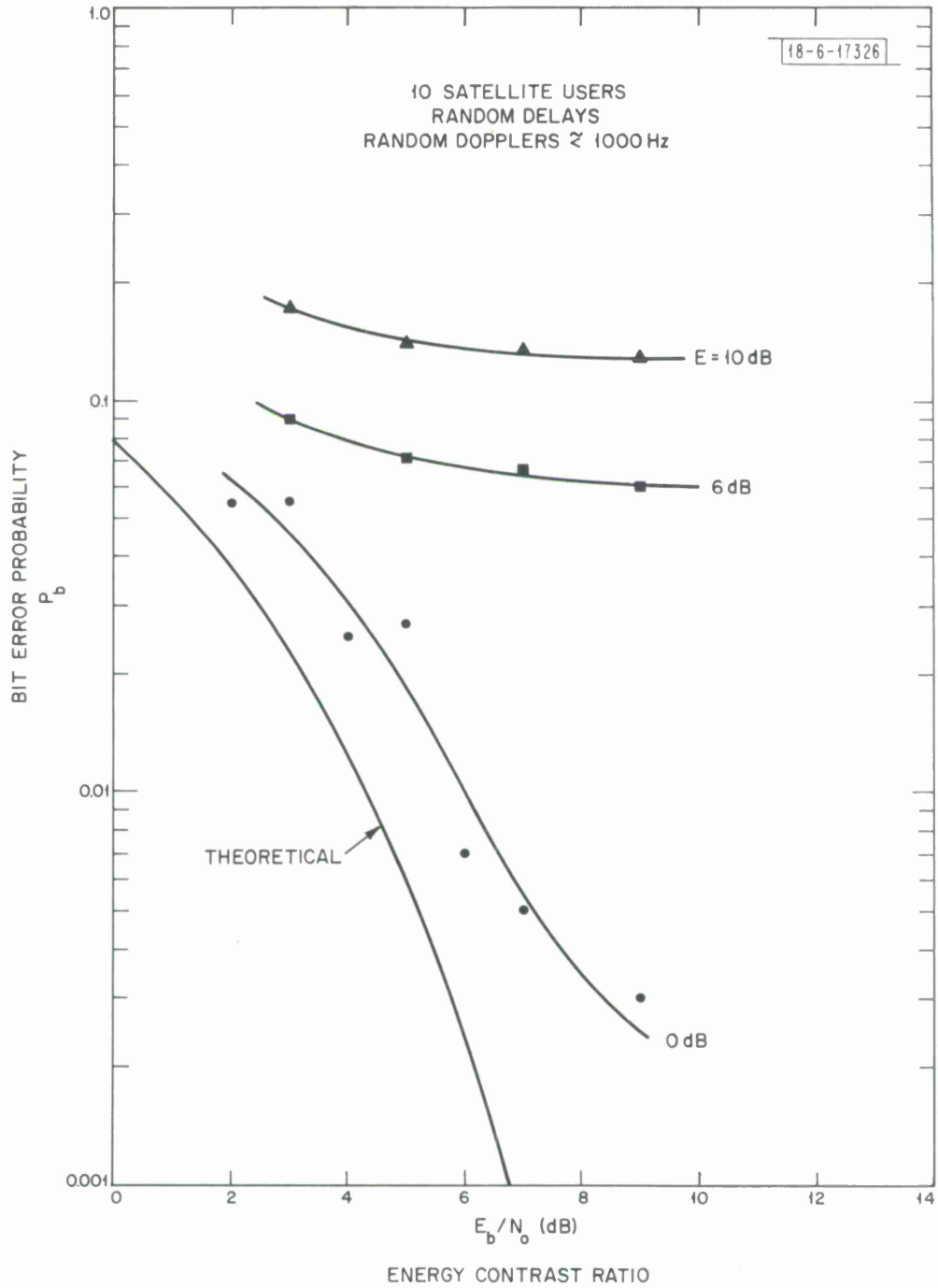

Fig. 4.8. Performance for uncoded 4800 bps minimum shift keying with center frequency spacing of 3750 Hz.

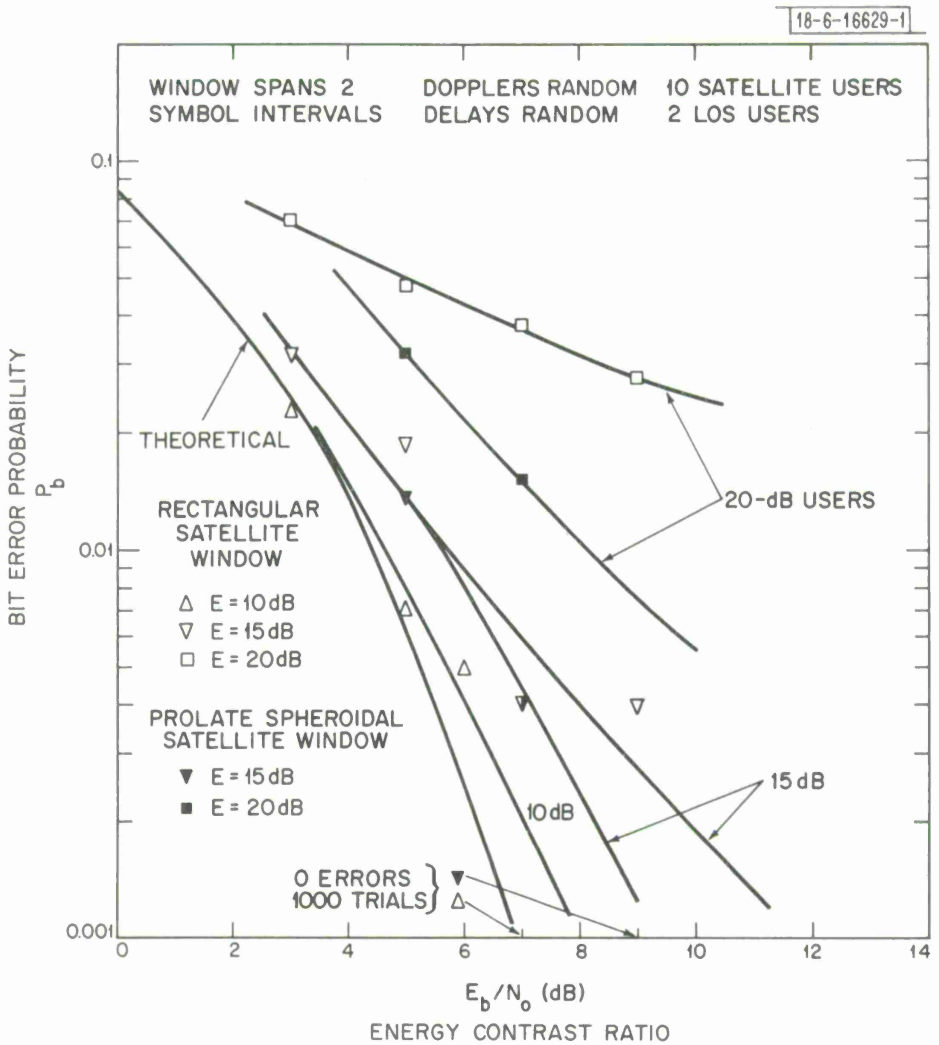

Fig. 4.9. Performance for uncoded 16k bps minimum shift keying with LOS users.

users below the 10 dB level. However, it appears that interfering users as large as 15 dB above the user being demodulated may be tolerable with a degradation of 2 to 5 dB from the ideal curve depending on whether or not the window is applied. Although the satellite window improves the performance considerably in the presence of 20 dB users, in this case the degradation from the ideal would be 4 to 10 dB.

When comparing coded QPSK with uncoded MSK on a bit error probability basis one must halve the ordinates and subtract L_t and the coding gain (see Section 4.5) from the abscissas of the QPSK curves. The results of such a comparison are given in Table 1.1.

Uncoded MSK is attractive because peak-power-limited transmitters can employ CE signaling, there is no ISI and hence no need for compensating filters at the satellite, and non-rectangular satellite windowing may be unnecessary. Of course, the convolutional decoders employing the Viterbi algorithm for the rate 1/2 code would also be absent from the MSK design. These advantages should be evaluated carefully before selecting the MSK scheme for implementation, however. Considering the complexity of the demodulation process in either QPSK or MSK as discussed in Section V the equipment savings for MSK may not be very important. Furthermore, coded QPSK should perform significantly better than MSK at the smaller error probabilities, e.g., $P_b = 10^{-5}$ as indicated in the next section.

4.5 Coding Gain for QPSK

QPSK simulations were performed only for uncoded QPSK but at the coded channel symbol rate of 16000 4-ary symbols per second necessary for a 16 kbps information rate and a rate 1/2 convolutional code. The actual coded QPSK

performance can be estimated from the simulated uncoded performance if the theoretical uncoded and coded performances are known. The usual technique [55,56] is to take a coding degradation (in increased E_b/N_o required for a given error probability) from the theoretical coded performance that is equal to the degradation of the simulated results from the theoretical uncoded performance at the same theoretical E_b/N_o reference value. This procedure will be illustrated by Fig. 4.10 for some of the QPSK simulations of Fig. 4.7 and the theoretical performance of a rate 1/2 constraint length 7 convolutional code over a coherent AWGN channel. For such a channel the bit error probability for convolutionally coded QPSK is identical to that of BPSK [57] just as the case for uncoded QPSK and BPSK.

Referring to Fig. 4.10 the theoretical coded performance for hard and soft decisions [42,54] indicates a coding gain, i.e., the improvement in E_b/N_o at a given error probability over the uncoded performance, of approximately 3 and 5 dB, respectively, over the theoretical uncoded performance for a bit error probability of 10^{-5}. The actual coded performance for the simulation is estimated as follows. For $P_b < 10^{-5}$ and 10 dB interfering users, for example, the theoretical soft decision coded E_b/N_o is about 4.8 dB. At this E_b/N_o the degradation of the 10 dB user simulation from the theoretical uncoded curve is approximately 2.0 dB. Therefore the predicted soft decision coding performance for 10 dB users is E_b/N_o = 6.8 dB. By roughly extrapolating the simulated 10 dB user curve it can be seen that the actual coding gain could exceed the theoretical 5 dB. It is generally true that the actual coding gain for a non-ideal modem exceeds that predicted from the theoretical curves. The coding gain for the hard decision case can be estimated in a similar fashion.

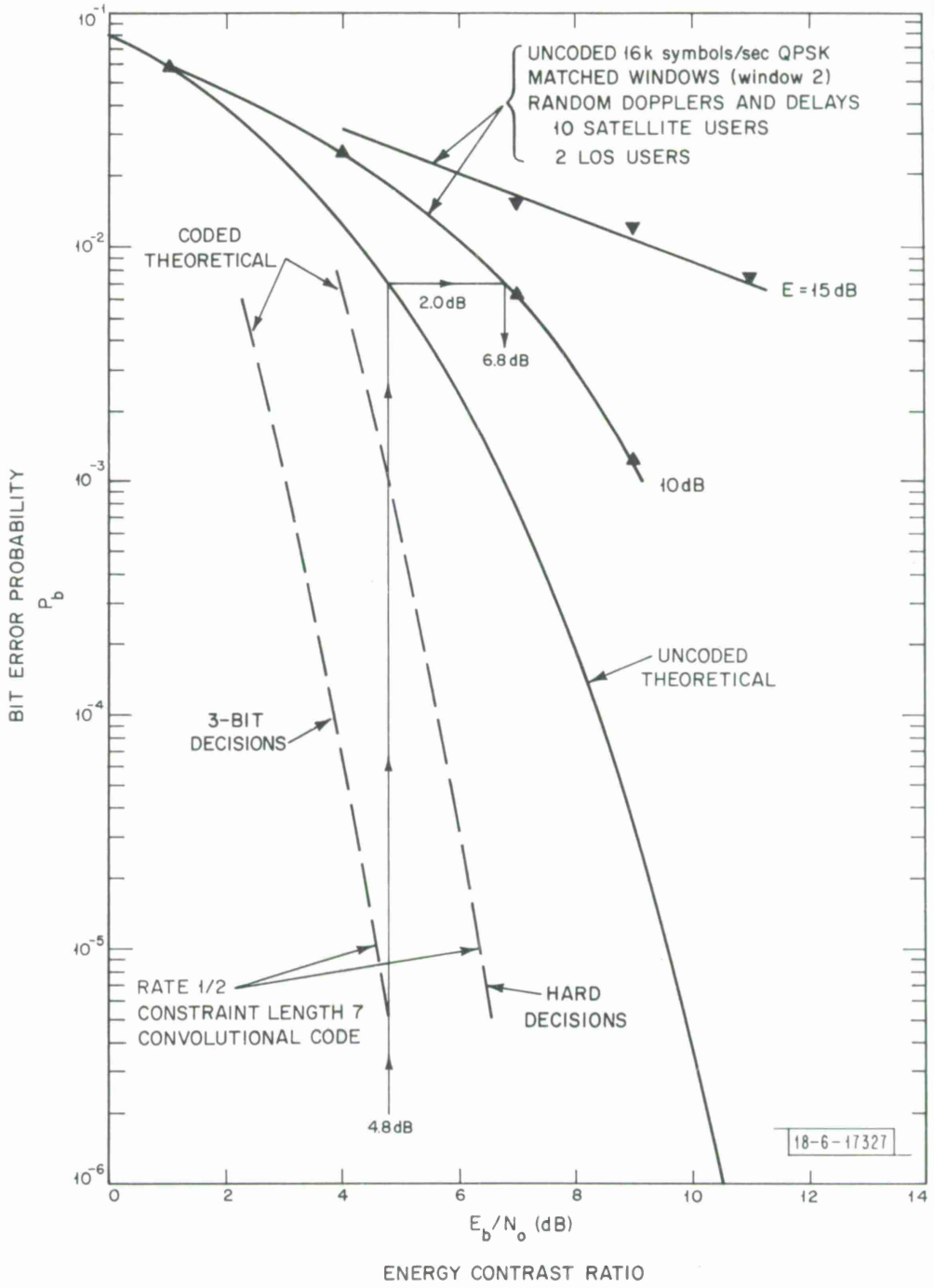

Fig. 4.10. Estimating coded QPSK performance using data of Fig. 4.7.

V. SATELLITE IMPLEMENTATION CONSIDERATIONS

The bulk of the satellite processing proposed in this report is represented in Fig. 5.1. The processor has four distinct components: 1) a sampler or analog to digital (A/D) converter; 2) some hardware which would window and store the data prior to its demodulation; 3) a digital demodulator which would implement either a series of discrete Fourier transform (DFT) calculations or a fast Fourier transform (FFT) algorithm; and 4) a bank of estimators which will be either simple digital filters or Viterbi decoders. In the first four of the six parts in this section the implementation requirements for each processing component are considered with respect to the various system configurations previously discussed. In the fifth part the number of real multiplications required for satellite processing is estimated. In the final part of this section, wordlength requirements are considered.

5.1 The Sampler

The need for a sampler is common to all of the digital schemes considered. To process 16 kbps data with 50 samples per symbol requires an A/D converter clock rate of 800 kHz which corresponds to a sampling interval of 1.25 μsec. Furthermore for both QPSK and MSK the received data are complex and thus two converters - one for the real part and one for the imaginary part - must be used. These schemes also put a slight extra burden on the analog portions of the system in that the modulator and demodulator must each provide two channels.

5.2 The Windowing Operation

Straightforward MSK requires no windowing at all so in that case this processing component may be omitted. However, satellite windows may be em-

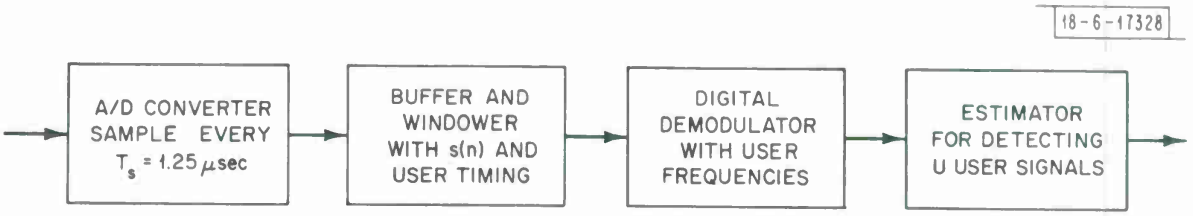

Fig. 5.1. Satellite processing components.

ployed with uncoded MSK if strong interfering users are present. If non-rectangular windowing is performed it must occur once per symbol interval, and it involves N_w multiplications. Since the window is real and the data complex, this requires that $2N_w$ real multiplications for QPSK (or MSK) and N_w real multiplications for BPSK be performed in T_c sec for each user demodulation channel. For $N_w = 100$ and $T_c = 62.5$ μsec this implies that a real multiplication be performed in 312.5 nsec for QPSK (or MSK) if one multiplier per user is allocated.

Alternately, 20 users might be handled with a high speed array multiplier capable of one real multiplication every 15.625 nsec. This may be pushing the current state of the art [58], however, and would be less reliable than using several time-shared slower multipliers. With synchronized user signals these multiplier requirements are eased by a factor U, the number of users, since then a single data window can be applied to all users simultaneously. $\frac{N_w}{2}$ words of storage are also required for the window function which is a real and even sequence.

5.3 The Digital Demodulator

Some form of digital demodulator is basic to all of the schemes considered. This component is the most complicated part of the system.

For QPSK and BPSK a number of DFT's equal to the number of users must be performed. If $f_u(n + n_u)$ represents the windowed sequence for the u-th user adjusted by the user delay n_u, and if $F_\zeta(\omega_u)$ represents the DFT output (ζ-th symbol, u-th user) then, cf. Eq. (2.4)

$$F_{\zeta}(\omega_u) = \sum_{n=0}^{N-1} f'_u(n+n_u)e^{-j\omega_u n} \tag{5.1}$$

where ω_u is the actual radial frequency of the received signal from the u-th user. Since n_u and ω_u are assumed known, Doppler and symbol timing tracking must be performed at the receiver.

The DFT of Eq. (5.1) can be implemented using one of the schemes shown in Fig. 5.2 for each ω_u. In Fig. 5.2a the output is sampled at the end of each symbol interval. It should also be noted that these output samplers for different users will not be synchronized unless the users are synchronized with respect to symbol timing.

The number of real multiplications can be approximately halved if the network of Fig. 5.2a is replaced by the Goertzel algorithm realization of Fig. 5.2b. The feedback operations are performed once per input sample, but the feedforward operation and the final sum is performed only at the end of each symbol interval at which time the storage elements are zeroed. For complex data this network must perform $2N_w + 8$ real multiplications every symbol interval plus some additions. Interestingly this is roughly the same requirement as for the windowing operation with unsynchronized users. An important difference is that even with synchronized users the discrete demodulation must be performed for each user whereas the windowing only needs to be performed once.

If the users are synchronized in time and frequency, Eq. (5.1) can be rewritten as

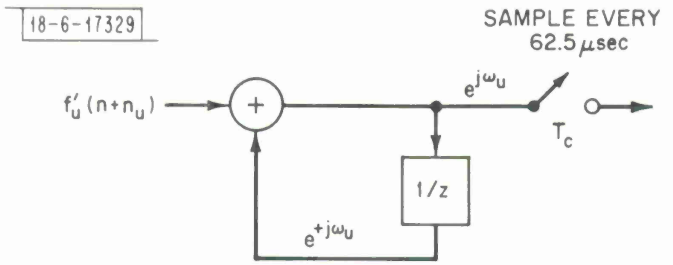

a. Straightforward implementation.

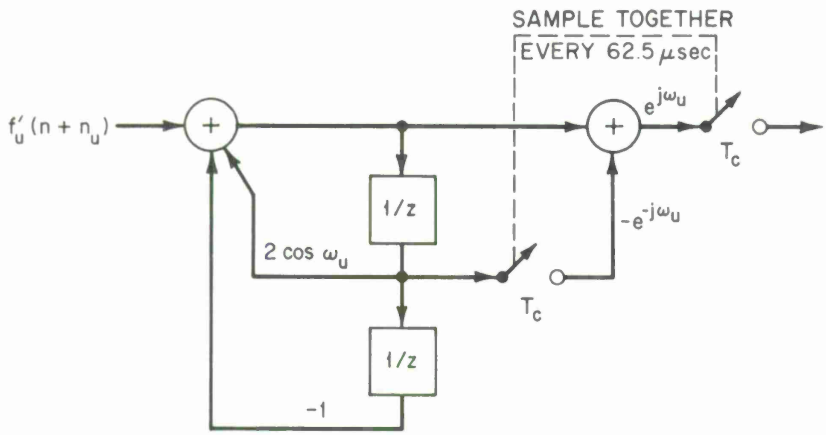

b. Realization requiring half the number of real multiplications of a.

Fig. 5.2. Discrete Fourier transformer for user u (Goertzel's algorithm).

$$F_\zeta(k) = \sum_{n=0}^{N-1} f''(n) e^{-j\frac{2\pi}{N_f}kn}, \quad k = 0,1,\cdots,N_f-1 \tag{5.2}$$

where $f''(n)$ is independent of u and where N_f represents the number of equally spaced frequency channels allocable. In contrast to previous discussion N_f is allowed to differ from N, the number of DFT input samples. In general $N > N_w > N_f$ ($N_f = 64$ for the simulations) and assuming that N_f divides N, in this case a faster implementation can be found by rewriting Eq. (5.2) as

$$F_\zeta(k) = \sum_{\ell=0}^{N_f-1} e^{-j\frac{2\pi k\ell}{N_f}} \sum_{m=0}^{N/N_f} f''(mN_f + \ell). \tag{5.3}$$

This implementation requires a few more additions but now requires only $2N_f + 4$ real multiplications for complex data. The total number of multiplications for all users can be approximately halved (again, if $N_f \approx N_w/2$) if users are assigned paired frequencies, i.e., if one user has frequency k/N_f another user should have frequency $\frac{N_f-k}{N_f}$. If both users are demodulated together the recursive computations implied by Fig. 5.2b can be shared and only the final multiplications must be performed twice.

Another alternative in the synchronized users case is to replace the bank of individual channel demodulators by a single box which performs an FFT of N_f points using Eq. (5.3) and in so doing demodulates all 64 channels (some of which may not be used) simultaneously. It would have to perform a 64-point FFT in 62.5 μsec, which is certainly technically feasible. Although the number of multiplications is not a totally reliable figure of merit, the FFT (radix 4)

would require at most 384 real multiplications. For QPSK the scheme in Fig. 5.2b modified for synchronized, paired users requires 140 real multiplications per pair of users. The FFT, therefore, becomes viable for 6 or more synchronized users.

For 16 kbps users at 25 kHz spacings the maximum Doppler shift is about ±4% of the 25 kHz spacing. In this case the implementation implied by Eq. (5.3) may be extremely close to that of Eq. (5.1), which implies that multiplications can be saved. Users cannot be paired, however, since this also requires time synchronization, so additional savings cannot be realized.

For purposes of comparison, an MSK demodulator requires $2N_c$ real multiplications per symbol interval per user ($N_c = 50$ for the uncoded MSK simulation). This computation could be performed using an FFT if the users were synchronized but a high order FFT would be necessary and only a limited number of its outputs would be used. The number of multiplications required with an FFT implementation will generally exceed the number required for a direct implementation, so the FFT approach would probably not be used.

5.4 The Estimators

Each estimator reduces any intersymbol interference (ISI) and makes a decision on the received symbol. In the coded case the Viterbi algorithm is applied to soft decisions to decode the transmitted information. Since this report is not concerned with coding nothing further will be said about the decoder. Although ISI does not occur for short ($N_w \leq 50$) windows or for MSK, this represents a rather insignificant hardware savings for these two cases. A 2-zero, 1-pole digital filter for removing ISI from QPSK requires eight real multiplications per symbol interval per user plus some additions, an extremely

modest requirement. If desired this linear filter could be time shared among the users rather easily with some buffering and control logic. For BPSK the number of multiplications would be halved.

For the Viterbi algorithm approach to combatting ISI, 4 real multiplications per symbol per user are required for the whitening filter and another 32 real multiplications are required per symbol per user by the Viterbi algorithm itself. Memory requirements for all of these schemes are modest.

5.5 Multiplications Required

The number of real multiplications required for the satellite processing components discussed in Sections 5.2, 5.3 and 5.4 are listed in Table 5.1. Referring to this table, unwindowed MSK takes 1/3 the multiplications of windowed MSK and less than 1/3 the multiplications of QPSK for unsynchronized users with insignificant Doppler shifts. With 20 synchronized users and insignificant Doppler shifts, QPSK requires about 1/3 the multiplications of MSK. Unwindowed MSK requires less than half the multiplications of either windowed MSK or QPSK for unsynchronized users when Doppler shifts are significant. Finally, with synchronized users and significant Doppler shifts, unwindowed MSK requires roughly 25% fewer multiplications. Thus, QPSK has fewer multiplications than MSK only when Doppler shifts are not significant and when users are synchronized.

5.6 Wordlength Requirements

Digital sequences correspond to sequences of b-bit numbers. Errors occur whenever numbers which require more than b bits for their representation must be quantized to b bits. Thus A/D converters and multipliers have a certain

TABLE 5.1

NUMBER OF REAL MULTIPLICATIONS PER SYMBOL REQUIRED FOR SATELLITE PROCESSING ($N_w = 100$, $N_c = 50$, $N_f = 64$, U = number of satellite users).

a. Unsynchronized Users, Dopplers Insignificant

modulation	operation			total
	windowing	demodulation	ISI filter	
QPSK	200U	132U	8U	340U
windowed MSK	200U	100U	0	300U
unwindowed MSK	0	100U	0	100U

b. Synchronized Users, Dopplers Insignificant

modulation	operation			total
	windowing	demodulation	ISI filter	
QPSK	200	384	8U	8U + 584
windowed MSK	200	100U	0	100U + 200
unwindowed MSK	0	100U	0	100U

c. Unsynchronized Users, Dopplers Significant

modulation	operation				total
	windowing	Dopplers	demodulation	ISI filter	
QPSK	200U	208U	208U	8U	624U
windowed MSK	200U	208U	100U	0	508U
unwindowed MSK	0	132U	100U	0	232U

d. Synchronized Users, Dopplers Significant

modulation	operation				total
	windowing	Dopplers	demodulation	ISI filter	
QPSK	200	208U	132U	8U	348U + 200
windowed MSK	200	208U	100U	0	308U + 200
unwindowed MSK	0	132U	100U	0	232U

amount of inherent noise associated with them. The energy represented by this noise decreases exponentially with increasing b. Thus by setting limits on the tolerable noise a required wordlength b can be determined. Hardware complexity also increases with b so the optimum b is the smallest one that will introduce tolerable error. Available hardware makes it particularly practical for b to be a multiple of 4 bits. The noise analysis performed to obtain the following results is based on a standard noise model [11,59].

Assuming a clip level magnitude of twice the standard deviation of the total A/D converter input of variance $2\sigma_t^2$, the effect of rounding to $b_{A/D}$ bits is to add complex white quantization noise of variance

$$2\sigma_q^2 = \frac{4(2\sigma_t^2)}{6}\, 2^{-2b_{A/D}} \tag{5.4}$$

to the input, where $(2^{-2b}A/D)/12$ is the variance of the quantization noise for a real input of unit magnitude. The number of quantization levels $2^{b}A/D$ should be chosen so that (5.4) is much less than the variance of the input without interfering users, namely,

$$2\sigma_s^2 = 2\sigma_n^2 + A^2 \tag{5.5}$$

where $2\sigma_n^2$ is the variance of the complex channel noise and A is the amplitude of the user being demodulated. If U-1 and E are the number and relative power level of the interfering users, then the desired condition on $b_{A/D}$ can be

written as

$$2^{2b_{A/D}} >> \frac{\frac{2}{3}(1+(1+(U-1)E)\frac{A^2}{2\sigma_n^2})}{1+\frac{A^2}{2\sigma_n^2}} . \qquad (5.6)$$

Replacing the user signal to channel noise ratio $A^2/2\sigma_n^2$ by $(E_b/N_o)(R/B)$, with $E_b/N_o = 10$, the user data rate to bandwidth ratio $R/B = 16/25$, and nine 15 dB interfering users, (5.6) becomes

$$2^{b_{A/D}} >> 12.8$$

or $b_{A/D} = 7$ is the required number of bits in the quantization.

If white noise with variance σ^2 is input to a DFT the output sequence is white with variance $N\sigma^2$, where N is the size of the DFT. The effect of multiplier quantization noise is equivalent to adding white noise at the input of the DFT with variance $\frac{1}{12}\,2^{-2b_{DFT}}$ where b_{DFT} is the wordlength in the DFT. The variance at the output of a 64-point DFT is therefore $\frac{64}{12}\,2^{-2b_{DFT}}$. Thus, if the input and output of the DFT are to have the same number of significant figures the internal wordlength of the DFT should contain an additional 3 bits.

One possible scheme then would be to use 8-bit A/D converters. The output of these can then be multiplied by an 8-bit window function and input to a 64-point DFT with internal wordlengths of 8 bits. The output of the DFT should then be significant to 4 bits. The wordlength used in the recursive filter or the Viterbi algorithm to remove ISI could be either 4 bits or 8 bits.

APPENDIX A

INDICES AND CHARACTERISTICS OF SIMULATION WINDOWS

WINDOW INDEX	WINDOW TYPE	WINDOW LENGTH N_w	WINDOW SPAN IN SYMBOLS NCW	CUTOFF FREQUENCY f_c(kHz)	MAXIMUM LOSS FOR PEAK-POWER-LIMITED TRANSMITTER L_t(dB)
0	CE	50	1	-	0
1	PS	64	3	12.5	2.61
2	PS	76	3	12.5	3.07
3	PS	88	3	12.5	3.44
4	PS	100	3	12.5	3.76
5	PS	128	3	12.5	4.36
6	DC	100	3	12.5	3.55
7	PS	50	1	12.5	1.96
8	PS	64	2	12.5	2.61
9	PS	76	2	12.5	3.07
10	PS	88	2	12.5	3.44
11	PS	100	2	12.5	3.76
12	DC	100	2	12.5	3.55
13	DC	150	3	12.5	4.50
14	DC	200	4	12.5	5.22
15	PS	76	3	8	1.89
16	PS	100	3	8	2.61
17	PS	128	3	8	3.26
18	PS	76	3	10	2.47
19	PS	100	3	10	3.20
20	PS	128	3	10	3.83
21	DC	50	1	12.5	15.4

APPENDIX B

INDICES AND CHARACTERISTICS OF ISI FILTERS

FILTER INDEX	WINDOW INDEX (transmitter/ satellite)	FILTER SYMBOL DELAY N_d	α_0	α_1	α_2	α_3	α_4	β_1	E_b/N_o+L_t (dB)*	USERS SPACED OR PACKED	MSE
2	1/1	1	-.1184	1.685	-.1190	-	-	.004683	11.45	SP	.085
25	2/2	1	-.2450	1.902	-.2496	-	-	.01756	10	SP	.096
26	3/3	1	-.3812	2.133	-.3963	-	-	.03671	10	SP	.108
27	4/4	1	-.5200	2.374	-.05530	-	-	.05984	10	SP	.123
29	1/1	1	-.1154	1.664	-.1163	-	-	.007156	10	PK	.096
30	2/2	1	-.2379	1.881	-.2429	-	-	.01889	10	PK	.105
31	3/3	1	-.3801	2.130	-.3951	-	-	.03675	10	PK	.109
32	4/4	1	-.5197	2.373	-.5527	-	-	.05983	10	PK	.123
35	5/5	1	-.8344	2.952	-.9322	-	-	.1104	10	PK	.166
43	0/13	1	-.5240	2.001	-.6006	-	-	.1003	10	PK	.153
46	2/2	1	-.2617	1.977	-.2674	-	-	.02071	13	PK	.061
49	3/3	1	-.4231	2.258	-.4407	-	-	.04098	13	PK	.060
53	4/4	1	-.5806	2.531	-.6195	-	-	.06699	13	PK	.072
54	4/4	2	.1526	-.6639	2.565	-.6700	.1648	-.01814	13	PK	.068
58	5/5	1	-.9660	3.240	-1.087	-	-	.1284	13	PK	.102
64	0/5	2	.0931	-.4485	1.860	-.4514	.09847	-.01207	13	PK	.098
84	1/1	1	-.1255	1.737	-.1265	-	-	.007689	13	PK	.057
89	15/15	1	-.3286	1.589	-.3473	-	-	.05385	13	PK	.081
90	18/18	1	-.3121	1.775	-.3244	-	-	.03801	13	PK	.067
93	12/12	1	-.7269	2.604	-.7674	-	-	.1005	13	PK	.096
94	12/12	2	.2523	-.9090	2.704	-.8851	.2593	-.03463	13	PK	.086
95	13/13	1	-1.315	3.872	-1.656	-	-	.2061	13	PK	.155
96	13/13	2	.5987	-2.037	4.489	-2.346	.9005	-.1190	13	PK	.126

* The listed values are the E_b/N_o's for a rectangular transmitter window (L_t = 0 dB) so that the channel Gaussian noise variance of each design is independent of the shape or length of the transmitter window.

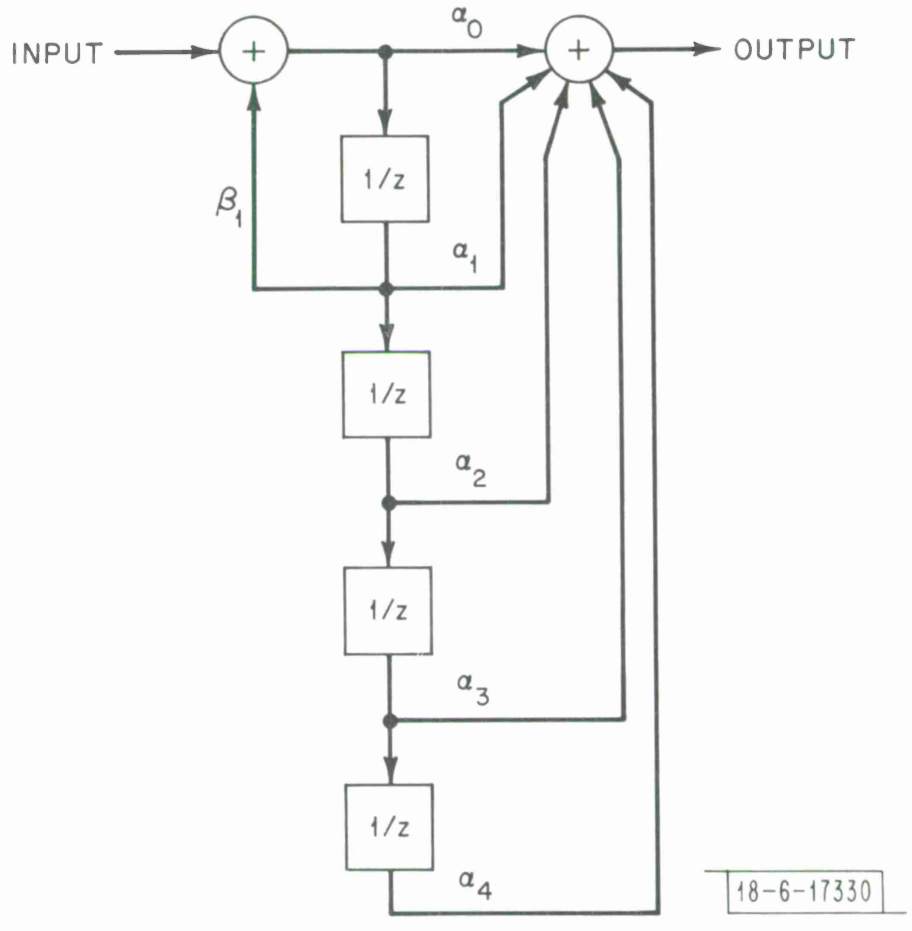

Fig. B.1. MMSE filter.

ACKNOWLEDGMENT

The authors gratefully acknowledge technical discussions with T. S. Seay, S. L. Bernstein, and K. S. Schneider, and the programming support of L. N. Weiner.

REFERENCES

1. B. Reiffen, L. J. Ricardi, L. W. Bowles, B. H. Hutchinson, C. W. Niessen, F. W. Floyd, and D. E. Weidler (LES-10 Design Group), "A Tentative Design for LES-10," Technical Note 1974-36, Lincoln Laboratory, M.I.T. (3 June 1974), DDC AD-919548-L.

2. R. J. Sims and R. P. Sherwin, "Communications Technology Trends in the DSCS," Proc. 3rd IEEE National Telecommunications Conference, San Diego, California, 2-4 December 1974, pp. 410-414.

3. R. E. Lyons and R. W. Parkinson, "System Design Considerations for the Future Defense Communications System," Proc. 2nd IEEE National Telecommunications Conference, Atlanta, Georgia, 26-28 November 1973, pp. 17D-1 to 17D-7.

4. J. N. Birch, "Low Bit Rate Voice Processors," Proc. IEEE Electronics and Aerospace Systems Convention, Washington, D. C., 7-9 October 1974, pp. 59-63.

5. J. J. Foshee, "Implementation Considerations with PSK Modulation," Proc. IEEE National Aerospace and Electronics Conference, Dayton, Ohio, 13-15 May 1974, pp. 346-349.

6. R. V. Groves and R. C. Beach, "Bandwidth Filtering Effects on PSK Modulation," Proc. IEEE National Aerospace and Electronics Conference, Dayton, Ohio, 13-15 May 1974, pp. 350-356.

7. K. S. Schneider, "Frequency Choice for Tactical Satellite Communications," Technical Note 1974-40, Lincoln Laboratory, M.I.T. (22 July 1974), DDC AD-783912/9.

8. B. E. White, "On the Close Packing of Unsynchronized FDM Waveforms," Technical Note 1975-34, Lincoln Laboratory, M.I.T. (14 October 1975).

9. K. Steiglitz, "The Equivalence of Digital and Analog Signal Processing," Inform. Contr. 8, 445-467 (1965); also in Digital Signal Processing, L. R. Rabiner and C. M. Rader, Eds. (IEEE Press, New York, 1972), pp. 7-19.

10. B. Gold and C. M. Rader, Digital Processing of Signals (McGraw-Hill, New York, 1969).

11. A. V. Oppenheim and R. W. Schafer, Digital Signal Processing (Prentice-Hall, Englewood Cliffs, New Jersey, 1975).

12. L. R. Rabiner and B. Gold, Theory and Application of Digital Signal Processing (Prentice-Hall, Englewood Cliffs, New Jersey, 1975).

13. M. E. Austin, "Decision-Feedback Equalization for Digital Communication Over Dispersive Channels," Technical Report 437, Lincoln Laboratory, M.I.T. (11 August 1967), DDC AD-664926.

14. S. Benedetto, E. Biglieri, and V. Costellani, "Combined Effects of Intersymbol, Interchannel, and Co-channel Interferences in M-ary CPSK Systems," IEEE Trans. Commun. COM-21, 997-1008 (1973).

15. L. Calandrino and G. Crippa, "Performance Analysis of PSK Radio Relay Systems," Alta Frequency 42, 572-582 (1973).

16. L. E. Eriksson, "Transmitter and Receiver Filters for Digital PAM Using Transversal Filters with Few Taps," IEEE Trans. Commun. COM-22, 1215-1225 (1974).

17. S. A. Fredricsson, "Optimum Transmitting Filter in Digital PAM Systems with a Viterbi Detector," IEEE Trans. Inform. Theory IT-20, 479-489 (1974).

18. F. E. Glave, "An Upper Bound on the Probability of Error Due to Intersymbol Interference for Correlated Digital Signals," IEEE Trans. Inform. Theory IT-18, 356-363 (1972).

19. T. S. Koubanitsas, "Performance of Multiphase CPSK Systems with Intersymbol Interference," IEEE Trans. Commun. COM-22, 1722-1726 (1974).

20. P. Monsen, "Adaptive Equalization of the Slow Fading Channel," IEEE Trans. Commun. COM-22, 1064-1075 (1974).

21. C. W. Niessen and D. K. Willim, "Adaptive Equalizer for Pulse Transmission," IEEE Trans. Commun. Technol. COM-18, 377-395 (1970).

22. O. Shimbo, R. J. Fang, and M. Celebiler, "Performance of M-ary PSK Systems in Gaussian Noise and Intersymbol Interference," IEEE Trans. Inform. Theory IT-19, 44-58 (1973).

23. J. G. Proakis, "Advances in Equalization for Intersymbol Interference," in Advances in Communication Systems Theory and Applications, Volume 4, A. J. Viterbi, Ed. (Academic Press, New York, 1975), pp. 123-198.

24. W. C. Lindsey and M. K. Simon, "Carrier Synchronization and Detection of Polyphase Signals," IEEE Trans. Commun. COM-20, 441-454 (1972).

25. S. A. Rhodes, "Performance of Offset-QPSK Communications with Partially-Coherent Detection," Proc. 2nd IEEE National Telecommunications Conference, Atlanta, Georgia, 26-28 November 1973, pp. 32A-1 to 32A-8.

26. S. A. Rhodes, "Effects of Noisy Phase Reference on Coherent Detection of Offset-QPSK Signals," IEEE Trans. Commun. COM-22, 1046-1055 (1974).

27. M. K. Simon and J. G. Smith, "Offset Quadrature Communications with Decision-Feedback Carrier Synchronization," IEEE Trans. Commun. COM-22, 1576-1584 (1974).

28. A. Viterbi, "Optimum Detection and Signal Selection for Partially Coherent Binary Communication," IEEE Trans. Inform. Theory IT-11, 239-246 (1965).

29. J. H. Halton and A. D. Spaulding, "Error Rates in Differentially Coherent Phase Systems in Non-Gaussian Noise," IEEE Trans. Commun. Technol. COM-14, 594-601 (1966).

30. R. W. Lucky, J. Salz, and E. J. Weldon, Jr., Principles of Data Communication (McGraw-Hill, New York, 1968).

31. C. L. Cuccia and W. E. Lee, "PSK and QPSK Modulation and Demodulation in Digital Satellite-to-Satellite and Satellite-to-Ground Links," Proc. AIAA 4th Communications Satellite Systems Conference, Washington, D. C., paper 72-532 (April 1972); in Communications Satellite Technology, Volume 33 of Progress in Astronautics and Aeronautics, (M.I.T. Press, Cambridge, Massachusetts, 1974), pp. 479-501.

32. J. G. Lawton, "Comparison of Binary Data Transmission Systems," Proc. 2nd National Conference on Military Electronics, Washington, D. C., 16-18 June 1958, pp. 54-61.

33. J. M. Wozencraft and I. M. Jacobs, Principles of Communication Engineering (Wiley, New York, 1965).

34. C. R. Cahn, "Performance of Digital Phase-Modulation Communication Systems," Trans. IRE, PGCS CS-7, 3-6 (1959).

35. S. A. Rhodes, "Effects of Hardlimiting on Bandlimited Transmissions with Conventional and Offset QPSK Modulation," Proc. 1st IEEE National Telecommunications Conference, Houston, Texas, 4-6 December 1972, pp. 20F-1 to 20F-7.

36. C. J. Wolejsza, Jr., A. M. Walker, and A. M. Werth, "PSK Modems for Satellite Communications," Proc. First Intelsat International Conference on Digital Satellite Communication, London, England, 25-27 November 1969, pp. 127-143.

37. R. deBuda, "Coherent Demodulation of Frequency-Shift Keying with Low Deviation Ratio," IEEE Trans. Commun. COM-20, 429-435 (1972).

38. R. deBuda, "About Optimal Properties of Fast Frequency-Shift Keying," IEEE Trans. Commun. COM-22, 1726-1727 (1974).

39. W. P. Osborne and M. B. Luntz, "Coherent and Noncoherent Detection of CPFSK," IEEE Trans. Commun. COM-22, 1023-1036 (1974).

40. F. E. Glave and A. S. Rosenbaum, "An Upper Bound Analysis for Coherent Phase-Shift Keying with Cochannel, Adjacent-Channel and Intersymbol Interference," IEEE Trans. Commun. COM-23, 586-597 (1975).

41. L. Palmer and S. Lebowitz, "Adjacent-Channel Interference Between Unfiltered and Filtered QPSK Signals," Proc. 9th IEEE International Conference on Communications, Seattle, Washington, 11-13 June 1973, pp. 31-25 to 31-29.

42. J. A. Heller and I. M. Jacobs, "Viterbi Decoding for Satellite and Space Communication," IEEE Trans. Commun. Tech. COM-19, 835-848 (1971).

43. S. Benedetto and E. Biglieri, "On Linear Receivers for Digital Transmission Systems," IEEE Trans. Commun. COM-22, 1205-1215 (1974).

44. J. W. Mark and S. S. Haykin, "Adaptive Equalisation for Digital Communication," Proc. IEE 118, 1711-1720 (1971).

45. R. Price, "Nonlinearly Feedback-Equalized PAM vs. Capacity for Noisy Filter Channels," Proc. 8th IEEE International Conference on Communications, Philadelphia, Pennsylvania, 19-21 June 1972, pp. 22-12 to 22-17.

46. J. Salz, "Optimum Mean-Square Decision Feedback Equalization," Bell Syst. Tech. J. 52, 1341-1373 (1973).

47. W. B. Davenport, Jr. and W. L. Root, An Introduction to the Theory of Random Signals and Noise (McGraw-Hill, New York, 1968).

48. G. D. Forney, Jr., "Maximum-Likelihood Sequence Estimation of Digital Sequences in the Presence of Intersymbol Interference," IEEE Trans. Inform. Theory IT-18, 363-378 (1972).

49. G. D. Forney, Jr., "The Viterbi Algorithm," Proc. IEEE 61, 268-278 (1973).

50. H. D. Helms, "Nonrecursive Digital Filters: Design Methods for Achieving Specifications on Frequency Response," IEEE Trans. Audio Electroacoust. AU-16, 336-342 (1968).

51. H. J. Landau and H. O. Pollak, "Prolate Spheroidal Wave Functions, Fourier Analysis and Uncertainty-II," Bell Syst. Tech. J. 40, 65-84 (1961).

52. D. Slepian and H. O. Pollak, "Prolate Spheroidal Wave Functions, Fourier Analysis and Uncertainty-I," Bell Syst. Tech. J. 40, 44-63, (1961).

53. E. Isaacson and H. B. Keller, Analysis of Numerical Methods (Wiley, New York, 1966).

54. A. R. Cohen, "Performance and Implementation of Viterbi Decoding," Proc. 7th Hawaii International Conference on System Sciences, Honolulu, Hawaii, 8-10 January 1974, pp. 204-206.

55. A. R. Cohen, "Practical Aspects of Convolutional Encoding with Viterbi Decoding," Proc. 11th IEEE International Conference on Communications, San Francisco, California, 16-18 June 1975, pp. 19-10 to 19-14.

56. I. M. Jacobs, "Practical Applications of Coding," IEEE Trans. Inform. Theory IT-20, 305-310 (1974).

57. A. R. Cohen and J. A. Heller, "Troposcatter Convolutional Encoder-Viterbi Decoder," Report ECOM-0248-73-1, U.S. Army Electronics Command, Fort Monmouth, New Jersey (June 1974).

58. B. Dunbridge, C. S. Miller and H. S. Ed Tsou, "Building Block Approach to Digital Signal Processing," Proc. IEEE Electronic and Aerospace Systems Convention, Washington, D. C., 7-9 October 1974, pp. 469-476.

59. A. V. Oppenheim and C. J. Weinstein, "Effects of Finite Register Length in Digital Filtering and the Fast Fourier Transform," Proc. IEEE 60, 957-976 (1972).

External Distribution List

The Defense Documentation Center
Attn: TISIA-1
Cameron Station, Bldg. 5
Alexandria, Virginia 22314 (2 copies)

Chief of Naval Operations (OP 941E)
Department of Navy
Washington, D. C. 20350

Computer Sciences Corporation
Systems Division 6565 Arlington Blvd.
Falls Church, Virginia 22046
Attn: Mr. C. C. Ingram
Mr. J. Burgess

Defense Communications Agency
8th and South Courthouse Road
Arlington, Virginia 22204
Attn: Dr. Frederick Bond
Dr. E. V. Hoversten
Dr. I. L. Lebow

Naval Electronics Laboratory Center
San Diego, California 92152
Attn: R.U.F. Hopkins Code 2420
Library

U.S. Naval Underwater Systems Center
New London Laboratory
Ft. Trumbull
New London, Connecticut 06321
Attn: Mr. John Merrill

Naval Postgraduate School
Electrical Engineering Dept.
Monterey, California 93940
Attn: Prof. John Ohlson, Code 52
Library

Commander
Naval Electronics Systems Command
Department of the Navy
Washington, D. C. 20360
Attn: PME-117
PME-106
PME-106-1, Capt. J. Pope
PME-106-1, Lt. Cdr. G. Burman
(6 copies)

NESC (continued)
Attn: PME-106-1, Lt. Cdr. C.J. Waylan
PME-106-1, J. Nooney
ELEX-03, T. B. Hughes
ELEX-00B, Dr. J. Lawson

U. S. Naval Research Laboratory
4555 Overlook Avenue, S. W.
Washington, D. C.
Attn: Code 5370, Mr. G. Goodman
Code 5400
Code 5404, Dr. W. S. Ament
Code 5406, Cdr. N. L. Wardle
Code 5430, Mr. Leavitt
Code 5430, Dr. LeFande

Department of the Navy
Command Support Programs, OP-094-H
Washington, D. C. 20350
Attn: Dr. R. Conley

Department of the Navy
Naval Telecommunication Division
OP-941T
4401 Massachusetts Avenue
Washington, D. C. 20350
Attn: Dr. McAllister

Department of the Navy
Naval Telecommunication Systems
Architect, OP-941N
4401 Massachusetts Avenue
Washington, D. C. 20350

Joint Tactical Communication Office (TRI-TAC)
Code TT-E-EX
Fort Monmouth, New Jersey 07703
Attn: Lt. Col. Ralph Maruca, Jr.

Director, Telecommunication & Command
& Control Systems (D/TACCS)
Pentagon, 3D-161
Washington, D. C.
Attn: Dr. K. L. Jordan
Mr. G. Salton
Capt. R. Runyon
Dr. J. Neil Birch

Institute for Defense Analysis
400 Army Navy Drive
Arlington, Virginia 22202
Attn: Dr. J. Aein

Air Force Systems Command, XRTS
Andrews Air Force Base
Washington, D. C. 20331
Attn: Maj. A. Baker

Headquarters, U.S. Air Force, RDS
Pentagon Room 5D-320
Washington, D. C.
Attn: Lt. Col. J. Carpenter

U.S. Army Satellite Comm. Agency
Fort Monmouth, New Jersey 07703
Attn: D. L. Labanca

The MITRE Corporation
Bedford, Mass. 01730
Attn: W. T. Brandon

ESD/DCKS
Headquarters
L. G. Hanscom Field
Bedford, Mass. 01730
Attn: M. Chaskin

G. E. LaVean
Defense Communications Engineering Center
Reston, Virginia

Allen Johnson
USAF-Avionics Lab.
AFAL/AAI
Wright-Patterson Air Force Base
Ohio

Dr. C. H. Chen
College of Engineering
Southeastern Mass. University
North Dartmouth, Mass. 02747

John H. Wittman
H. Gibbons
T. A. Schonhoff
GTE Sylvania
77 "A" Street
Needham Heights, Mass. 02194

Prof. D. L. Snyder
Biomedical Computer Laboratory
Washington University School of Medicine
700 S. Euclid Avenue
St. Louis, Missouri 63110

Robert E. Morley, Jr.
Electrical Engineering Department
Washington University
Box 1127
St. Louis, Missouri 63130

Prof. J. M. Wozencraft
Room 35-208
Electrical Engineering Department
Massachusetts Institute of Technology
Cambridge, Massachusetts

Prof. R. M. Mersereau (5 copies)
School of Electrical Engineering
Georgia Institute of Technology
Atlanta, Georgia

UNCLASSIFIED

SECURITY CLASSIFICATION OF THIS PAGE *(When Data Entered)*

REPORT DOCUMENTATION PAGE		READ INSTRUCTIONS BEFORE COMPLETING FORM
1. REPORT NUMBER ESD-TR-75-329	2. GOVT ACCESSION NO.	3. RECIPIENT'S CATALOG NUMBER
4. TITLE *(and Subtitle)* A Bandwidth Conserving Approach to Multiple Access Satellite Communication for Mobile Terminals		5. TYPE OF REPORT & PERIOD COVERED Technical Note 6. PERFORMING ORG. REPORT NUMBER Technical Note 1975-26
7. AUTHOR*(s)* White, Brian E. and Mersereau, Russell M.		8. CONTRACT OR GRANT NUMBER*(s)* F19628-76-C-0002
9. PERFORMING ORGANIZATION NAME AND ADDRESS Lincoln Laboratory, M.I.T. P.O. Box 73 Lexington, MA 02173		10. PROGRAM ELEMENT, PROJECT, TASK AREA & WORK UNIT NUMBERS Program Element No. 33109N
11. CONTROLLING OFFICE NAME AND ADDRESS Naval Electronic Systems Command Department of the Navy Washington, DC 20360		12. REPORT DATE 17 December 1975 13. NUMBER OF PAGES 120
14. MONITORING AGENCY NAME & ADDRESS *(if different from Controlling Office)* Electronic Systems Division Hanscom AFB Bedford, MA 01731		15. SECURITY CLASS. *(of this report)* Unclassified 15a. DECLASSIFICATION DOWNGRADING SCHEDULE

16. DISTRIBUTION STATEMENT *(of this Report)*

Approved for public release; distribution unlimited.

17. DISTRIBUTION STATEMENT *(of the abstract entered in Block 20, if different from Report)*

18. SUPPLEMENTARY NOTES

None

19. KEY WORDS *(Continue on reverse side if necessary and identify by block number)*

communications satellite
mobile terminals
BPSK modulation
FDMA
Navy communications
uplink bandwidth
MSK modulation
data windows
QPSK modulation
MPSK digital system

20. ABSTRACT *(Continue on reverse side if necessary and identify by block number)*

The problem of efficiently packing many mobile user signals into the available UHF uplink bandwidth of an advanced communications satellite is considered. The basic approach is FDMA with QPSK modulated data streams individually modified by spectral shaping using data windows.

From extensive computer simulations it is concluded that with relatively little degradation 20 unsynchronized 16 kbps satellite users can be packed into a 500 kHz uplink bandwidth that is shared with terrestrial LOS allocations. Alternatively, 7 unsynchronized 2400 bps users can occupy a 25 kHz bandwidth. Signal strengths may vary by as much as 10 to 15 dB at the satellite without the need for transmitter power control.

DD FORM 1 JAN 73 1473 EDITION OF 1 NOV 65 IS OBSOLETE

UNCLASSIFIED

SECURITY CLASSIFICATION OF THIS PAGE *(When Data Entered)*